Institut für Fertigungstechnik und Werkzeugmaschinen

Prof. Dr.-Ing. B. Denkena

Studienarbeit

Experimental analysis of chip formation when hard machining as a function of the shape of the cutting edge

Verfasst von:

Herr Guillermo Andrés Iglesias

Matrikel-Nr.: 10054450

Betreut von:

M. Sc. Arnd Christian Heckemeyer

Erstprüfer:

Prof. Dr.-Ing. Berend Denkena

Garbsen, den 23. März 2023

Abstract

Thema der Arbeit: Experimental analysis of chip formation when hard machining as a function of the shape of the cutting edge

Erstellt von: Herr. Guillermo Andrés Iglesias

Matr.-Nr. 10054450

Kenn-Nr.: 22-P 5538 / 3-Hec

Abgabedatum: 23. März 2023

Betreut von: M. Sc. Arnd Christian Heckemeyer

Due to the high resulting thermomechanical load, the machining of hardened steels is challenging for the applied cutting material. Therefore, polycrystalline cubic boron nitride (PcBN) is predominantly used. In order to stabilize the cutting edge, a specific adjustment of the cutting edge microgeometry has also shown to be effective, influencing both the chip formation and the tool load stresses. The preparation of the cutting edge can be carried out by various methods, such as abrasive brushing or plunge face grinding. While brushing results in a continuous cutting edge rounding, this is approximated by multiple chamfers in plunge face grinding. The chip formation, cutting forces and surface roughness of the machined surface are therefore determined by the size and shape of the microgeometry. However, the exact relationships between cutting edge shape and chip formation are currently unknown and the subject of ongoing research.

Erklärung

Hiermit versichere ich, dass ich die vorliegende Ausarbeitung ohne fremde Hilfe angefertigt habe und mich dabei anderer als der von mir angegebenen Hilfsmittel nicht bedient habe.

Hannover, den 23. März 2023

_____

Unterschrift

Contents

List of figures

List of tables

List of abbreviations

Abbreviation	Description
FEM	Finite element method
GBS	Grain boundary sliding
HP-HT	High-pressure high-temperature synthesis
HRC	Rockwell hardness C
HV	Vickers hardness
PcBN	Polycrystalline cubic boron nitride
PCD	Polycrystalline diamond
SiC	Silicon carbide

List of symbols

Symbol	Description	Unit
α	Clearance angle	Deg
φ	Apex angle	Deg
γ_f	Flank angle	
γ_r	Rake angle	Deg
Δr	Profile flattening	µm
a_p	Depth of cut	mm
f	Feed rate	mm/rev
G_s	Degree of segmentation	
h_{max}	Maximum uncut chip thickness	mm

K	Form factor between S_γ and S_α	
R_ε	Nose radius	mm
R_a	Average of the profile height measuring from the mean line	µm
R_z	Maximum of the profile height measuring from the mean line	µm
S_α	Segment of the cutting edge corresponding to the flank face	µm
S_γ	Segment of the cutting edge corresponding to the rake face	µm
v_c	Cutting speed	m/min

1 Introduction

During the last few decades, machining of hardened steels with geometrically defined cutting edges has largely replaced grinding in the manufacturing industry. This has been possible due to the development of new cutting tools capable of withstanding the high thermomechanical demands that characterize hard machining. These types of tools are polycrystalline cubic boron nitride inserts (PcBN) that have allowed the expansion of hard turning, achieving similar results to grinding with lower operating costs and greater versatility. Metal turning with a defined cutting edge has as a characteristic a directly contact between the workpiece and the tool edge, therefore, exist a directly relation between the size and shape of the cutting edge and the quality of the final workpiece. Also, tool wear and chip formation will be genuinely affected by the cutting edge. All these interactions are not exactly known for hardened steels and are the subject for this research.

The objective of this thesis is to analyse the influence of the size and shape of the cutting edge in cutting forces, chip formation and surface roughness when turning AISI 52100 hardened steel, commonly used in the industry to manufacture bearings. The process forces and surface roughness of the final workpiece have been monitored during the process and the chip section has been analysed in order to state relations between them and tools microgeometry. On the other hand, two different types of cutting edge preparation have been used, brushing, which a continuous rounding can be achieved, and grinding, which resulted in a discontinuous rounding approximated by microchamfers. In addition, the differences in chip formation, cutting processes and surface quality for both of edge preparations will be studied.

Within the scope of this thesis, the relation between process parameters (cutting speed, feed rate and depth of cut) and process forces has been thoroughly analysed for the different edge microgeometries. A force model has been developed to predict cutting forces as a function of the engagement area, which exist a linear relation between it and the feed rate and cutting depth. Therefore, many experiments have been carried out varying the cutting parameters to obtain different values with the aim of fitting a model to the obtained results.

2 State of art

2.1 Turning processes

DIN 8580 classifies manufacturing processes into six different categories: cutting, forming, joining, coating, changing substance properties and casting. This work relates to cutting methods that can be defined as a material removal process using a tool tip that has to be harder than the workpiece material. In turning operations, the workpiece is rotating while the tool is describing a linear feed motion along the workpiece axis as displayed in Figure 2.1.

Moreover, there are many other operations performed on a lathe, such as facing, that the feed direction is perpendicular to the workpiece axis or drilling where the feed direction is lengthwise. Other examples for machining are grooving, parting, drilling or threading.

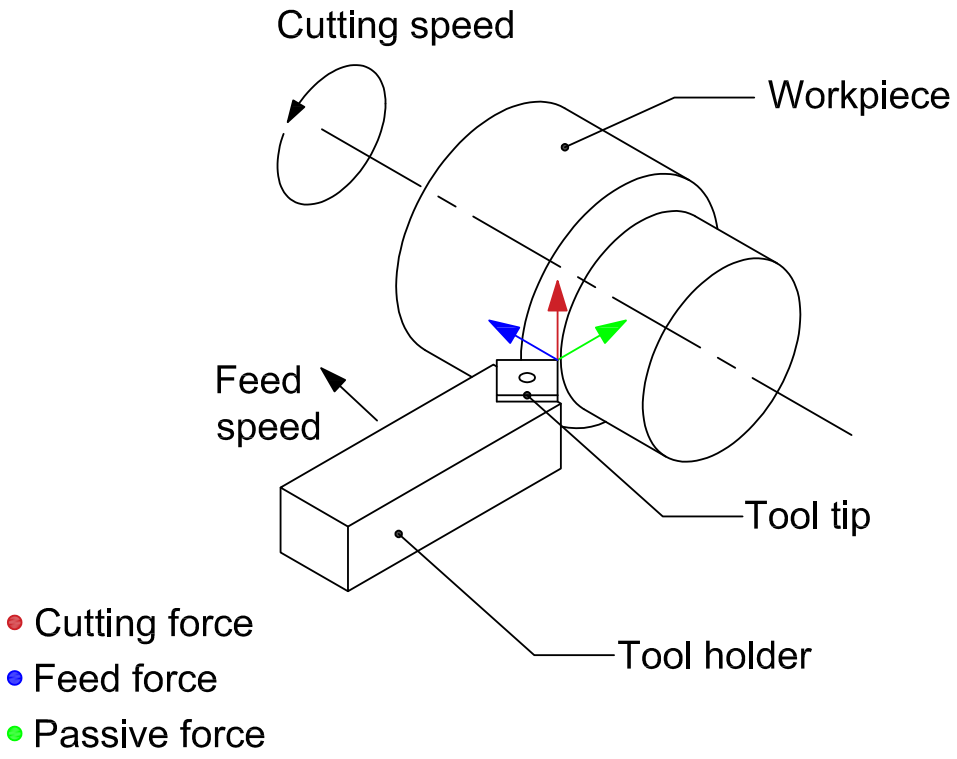

Figure 2.1: Turning process [DENK11].

The quality of the final piece depends on multiple factors, for example, the stiffness of the whole machine is decisive in the surface roughness and dimensional accuracy. On the other hand, the micro and macrogeometry of the tool can greatly influence the parameters mentioned above and also the process forces and the tool life are

important factors. The macroscopic features involve, for example, the corner radius and the clearance and rake angle. Regarding to the microgeometry, the size and shape of the cutting edge influences the factors mentioned above.

The process force can be divided into three components as passive, feed and cutting force. The cutting force acts in the tangential direction, and it is directly related to the power of the spindle motor. The feed force, which acts in the longitudinal direction, and it is linked with the feed motors, and finally, the passive force that is related to the dimensional tolerances of the achieved piece. It is detailed in Figure 2.1.

2.2 Machining of hardened steel

Hardened steel is medium or high carbon content steel that has been subjected to a heat treatment such as quenching hardening. This process consists of heating the steel above the transformation temperature and subsequent cooling, during which the martensitic lattice is formed. The martensitic lattice provides the high hardness but also for an embrittlement of the material due to the microstructure created and it must be tempered which allows to set a balance of hardness and toughness. Tempering process is used to increase toughness of a steel alloy and it is done by heating the workpiece below the critical point and then let it cool in the air. As mentioned above, this action reduces the material hardness in favour of increasing the fracture toughness which makes it more suitable for some industrial applications. One major application of hardened steels are bearings. Where the steel grade AISI52100 is commonlyº used.

During the last decades machining of hardened steel using grinding operations has been more suitable process to achieve high quality surface roughness and dimensional accuracy. Otherwise, turning instead of grinding has established itself as the most suitable form for machining these types of materials due to the fact that it is possible to perform different operations like internal and face turning without moving the workpiece what is not possible in most of the cases in grinding operations. On the other hand, the possibility of machining without the use of any coolant is other advantage because this fluid needs power for its supply, also is difficult to recycle and has a considerable effect on the environment. [GODO11]

The development of new very hard tool materials, like ceramics and PcBN (Polycrystalline Cubic Boron Nitride) has contributed to the expansion of hard turning techniques, due to their high thermal and chemical stability. In terms of tool life, in turning of hardened steel the principal type of wear is crater and flank wear and it can contribute to dimensional errors and bad surface roughness. Moreover, the tool wear

influences the forces involved in the turning process specially the passive forces acting in the radial direction, cutting and feed forces are also influenced.

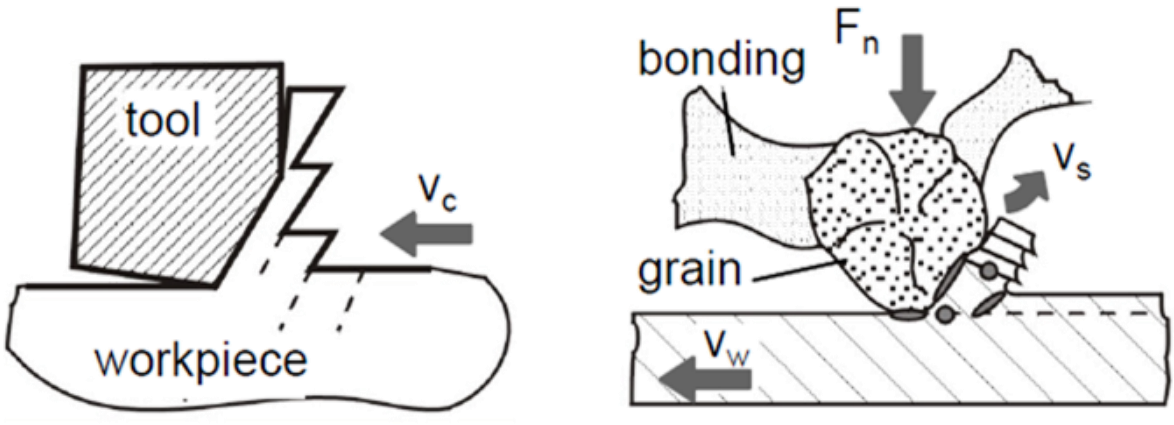

Figure 2.2: Turning process (left) and grinding process (right) [KLOC05]

About process forces, Bouacha et al. (2010) [BOUA10] performed force measurements when turning hardened steel (AISI 52100 used for bearings) with a hardness of 64 HRC. They tested different cutting speeds with constant feed rate and depth of cut (f = 0.08 mm/rev, ap = 0.3 mm) and PcBN tools were used for the experiments. They also delimited the hard turning domain for all the steels with a hardness higher than 50 HRC.

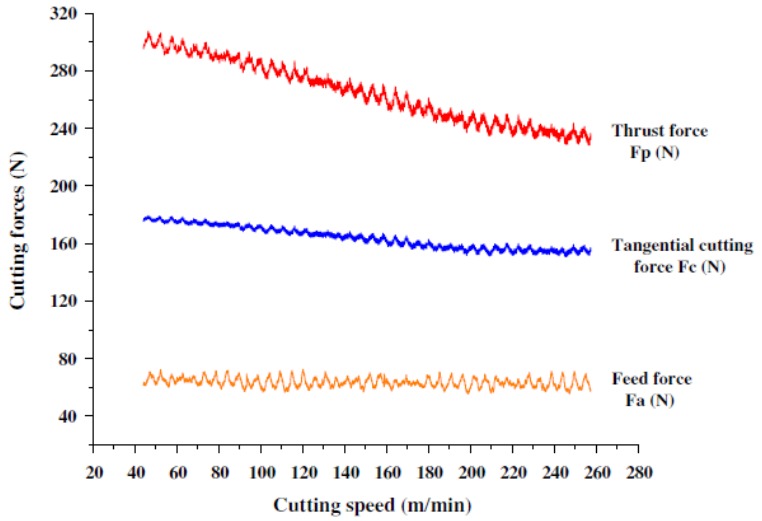

Figure 2.3: Cutting forces as a function of the cutting speed [BOUA10]

As can be seen in Figure 2.3, the thrust force (direction perpendicular to the workpiece axis, in this document called passive force) is the bigger component regarding of the process parameters and decrease with the increasing cutting speed. The feed force is the lowest and has no variation with the constant feed rate. In regard to the tangential cutting force showed a slight decrease with the increasing cutting speed. It can be explained due to the softening effect that appears in the workpiece caused by the higher temperatures reached around the tool edge when increasing the cutting speed.

2.3 PcBN tools

Boron nitride is a heat and chemical resistant material made up of nitrogen and boron. It has different crystalline forms; the hexagonal form is the most stable and soft and it has a structure analogous to graphite. The one used in machining is the cubic form, which has a structure similar to diamond which provides high hardness. Furthermore, the cubic phase has a high stability against chemical reactions. This it is the reason why it is appropriate for machining of hard materials. As it is known, CBN has a lower hardness than diamond, but it is more suitable for iron or nickel-based alloys due to the solubility of diamond in these materials. Furthermore, diamond tends to recrystallization to graphite at high temperatures. The physical and mechanical properties are described in the following table. It must be noted that PcBN is a combination of cBN and the binder phase. Therefore, the properties may vary depending on the of cBN content of the tool.

PcBN tools mostly consist of a carbide base body onto which a PcBN insert has been brazed. The most widespread technique for manufacturing PcBN tools is the high-pressure high-temperature synthesis (HP-HT). This process is used in the industry but also is in constant development for make the tools cheaper and reduce the amount of energy needed to carry them out with environment-friendly techniques due to the high pressures and temperatures needed (around 40 kbar and 1500 °C) [ABRA93].

This type of tools also has excellent wear resistance for ensure enough tool life for industrial applications. De Godoy et al. (2011) [GODO11] concluded that PcBN tools perform better than ceramic tools due to their wear resistance and longer tool life for machining of hardened steels in continuous and interrupted cutting. Also, PcBN tools achieved better surface roughness. Therefore, nowadays at the manufacturing industry PcBN inserts are the most used tools for machining hardened steel.

Usually, PcBN tools are divided in two types according to the PcBN content. The ones with high content (PcBN-H) perform better for interrupted cutting due to their superior

toughness what allows the tool to withstand the hits when turning discontinuous surfaces, PcBN-H inserts usually use metallic binders like cobalt. On the other hand, low content PcBN tools (PcBN-L) are more suitable for continuous cutting due to their higher chemical and thermal stability comparing to the PcBN-H, despite of the lower hardness and toughness due to the lower concentration of PcBN and different binder they use (normally ceramic binders such as titanium nitride). These properties are needed for continuous cutting owing to the high temperatures reached in this type of processes. For interrupted cutting is not needed this extremely high heat resistance because the tool can cool down itself in the periods that the tool is not in contact with the workpiece.

Table 1: Physical and mechanical properties of PcBN [CHOU99]

	Density (kg/m^3)	**Knoop hardness (GPa)**	**Fracture toughness ($MPa\ m^{1/2}$)**	**Young's modulus (GPa)**	**Poisson's ratio**	**Thermal conductivity (W/mK)**	**Coefficient of thermal expansion (10^{-6}/K)**
PcBN-H	3100	31.6	6.3	680	0.22	100	4.9
PcBN-L	4280	27.5	3.7	587	0.15	44	4.7

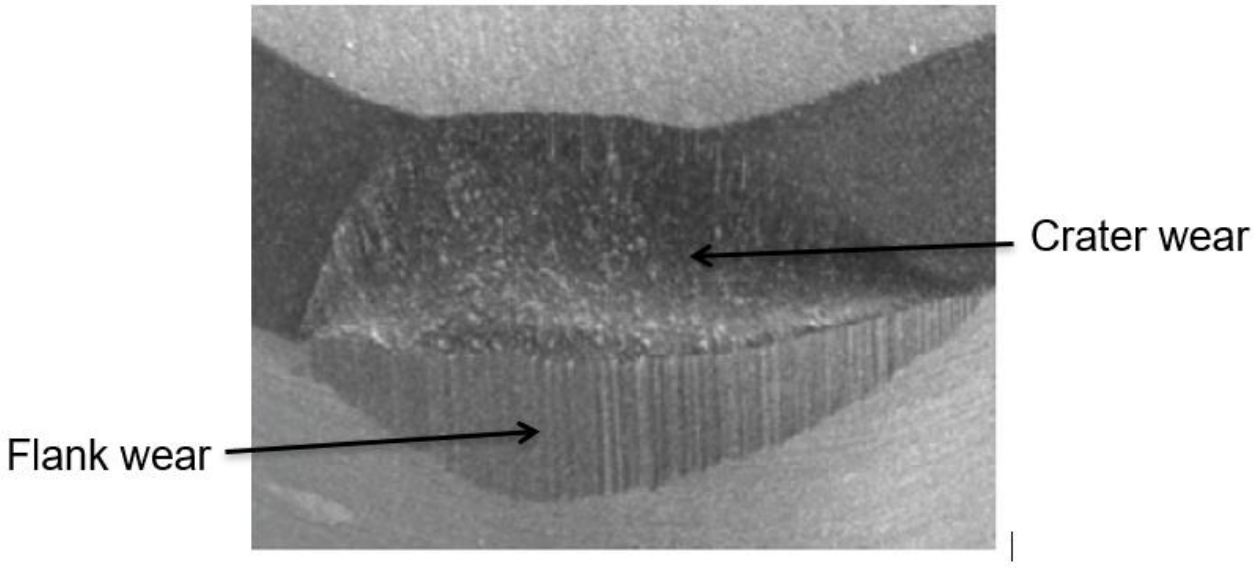

Figure 2.4: Typical tool wear while turning hardened steel [SADI12]

As has been previously commented, PcBN tools are normally used for hardened steel machining, many authors have investigated about wear development of these processes. Sadik (2012) [SADI12] showed that the most important wear mechanisms are abrasive and diffusion wear regardless of the type of hardening method. In the picture below (Figure 2.4) it can be seen the crater and flank wear of PcBN tool which has been used for turning DINX100CrMoV51 (through hardened steel) with a hardness of at least 59 HRC and a composition of 0.95% of carbon. For other types of hardening (case and induction) the same wear mechanisms were observed.

Chou et al. (1999) [CHOU99] conducted experiments testing low and high content PcBN tools for turning interrupted cutting surfaces. The workpiece was made of hardened steel with about 60 HRC. The results showed that high content tools performed better achieving longer tool life for low cutting speeds reducing it as the cutting velocity increased. It was observed that tool life is highly influenced by cutting speed and frequency of interruptions. The main influence in tool life for PcBN-H is the high temperatures reached due to the increasing cutting speed. As has been previously mentioned, high content tools have lower thermal and chemical stability due to the solubility of the metal binder in the workpiece material, compared to the low content inserts. Respecting low content PcBN tools, the author concluded that medium cutting speeds are the most suitable for achieving the longest life minimizing the tool wear. In terms of wear development, crater and flank wear were the only ones observed.

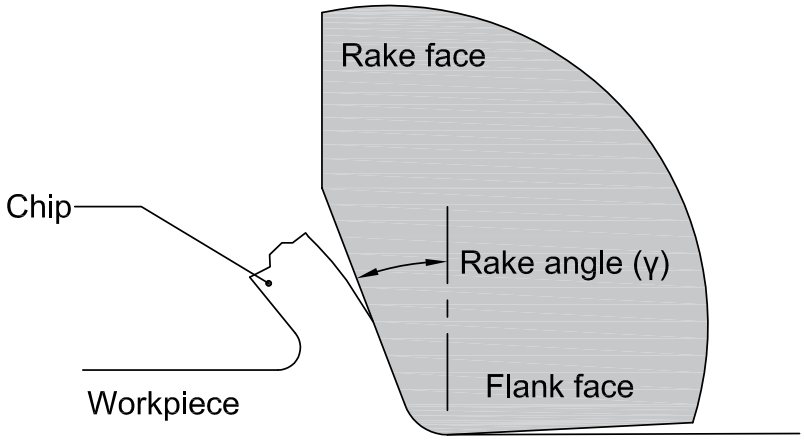

Figure 2.5: Geometry of the cutting tool [ZHOU03]

Other aspect that influences the perform of PcBN tool is the microgeometry (described in next section) and macrogeometry. One important parameter of tool macrogeometry is the rake angle. Numerous authors studied its effect on wear and perform of PcBN cutting tools [ZHOU03] concluding that wedge stability will increase with an increase

of chamfer angle and thus leading to a superior tool life. In Figure 2.5 it is described the typical negative rake angle used in PcBN tools for hard machining.

2.4 Cutting edge microgeometries

The influence of the cutting edge microgeometry for machining has been investigated by numerous authors during last decades concluding that exist a great influence in the process forces, surface roughness and tool life. Due to this it is necessary to investigate about cutting edge microgeometries and developed new techniques for the edge preparation. Several experimental investigations and simulations carried out during the last years have tried to describe the influence of the cutting edge size and shape in machining processes. In general terms, the biggest microgeometries obtain the highest thermal load acting on the tool, in contrast with the internal stresses of the tool which decrease with the increasing size of cutting edge microgeometry.

Regarding to cutting edge preparation, exist multiple techniques for achieving the desired microgeometry. They include brushing, grinding, abrasive jet machining or laser machining among others. Some of them like brushing, can produce a continuous rounding of the cutting edges whereas other processes like grinding, generate an approximation of a rounded edge using multiple microchamfers. This topic will be covered in detail in the chapter about cutting edge preparation.

In order to define the cutting edge microgeometry of a certain tool, is normally used an ideal arc with radius of r_β. However, this method only works for symmetrical edges and not for the asymmetrical ones. Due to that, Denkena et al. [DENK05] developed a new technique based in a form factor method to define both types of cutting edges. The parameters used are S_α, S_γ, Δr and φ (see Figure 2.6). S_α and S_γ are the segments corresponding to the flank and rake face respectively, Δr is the profile flattening and φ is the apex angle. A complete definition of shape and size of cutting edges, is obtained using these parameters. This allows the researchers to compare different microgeometries analysing the effects produced during machining operations. However, some disadvantages appear with this method because accuracy depends on the position and direction of the tangent segments used to measure S_α and S_γ. Precision is subjected to the number of points used for the calculation at both faces of the edge. In addition, the location of the separation of S_α and S_γ tangents is highly dependent on the fitting area of a given face used to evaluate the tangent. Therefore, the operator plays a fundamental role in evaluating if there is a correct fit in the tangents obtained in the measurement. [DENK14]

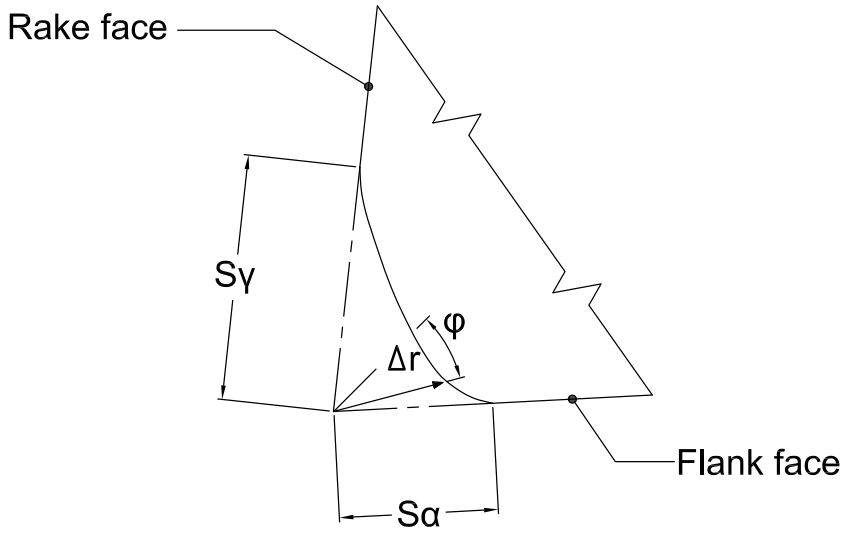

Figure 2.6: Form factors for defining cutting edges

As mentioned above, the size and shape of the cutting edge strongly influence the performance and behaviour of the tool during the machining operations. Tool preparation processes can achieve two different types of microgeometries. These are symmetrical and asymmetrical geometries as can be seen in Figure 2.7 and Figure 2.8. The form factor K describes the ratio between S_γ and S_α quantifying the value of the asymmetry. K = 1 defines a symmetrical profile and K ≠ 1 is used for the non-symmetrical ones.

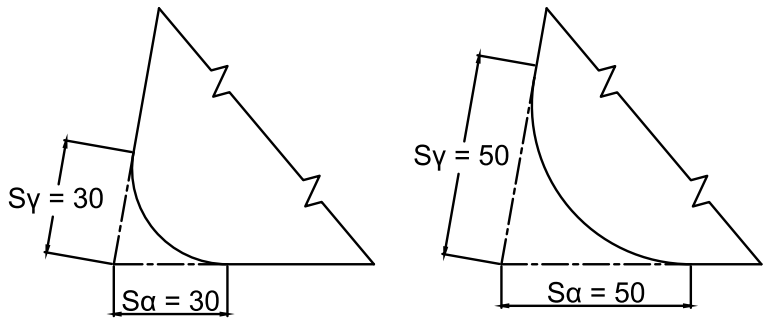

Figure 2.7: Symmetrical cutting edge profiles (K=1)

The shape of the cutting edge influences the stagnation point, where the material split in two flows, one that goes over the tool generating the chip and another that is pressed under the flank face generating the new surface on the workpiece. The stagnation zone will be bigger with the increase of the cutting edge microgeometry (S_α and S_γ) causing an increasement in the process forces. Also, it can affect the surface roughness and

residual stresses of the final workpiece due to the ploughing effect of the tool, which is caused by the amount of material flowing underneath of the flank face.

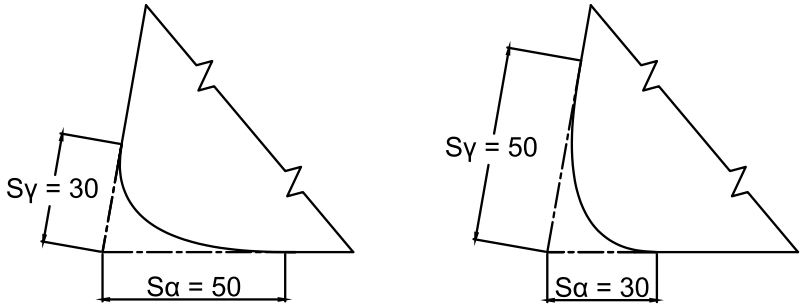

Figure 2.8: Asymmetrical cutting edge profiles (K=0.6, left and K=1.66, right)

Denkena et al. [DENK21] performed numerical and experimental analysis when machining hardened steel (AISI 52100) using ground cutting edges. They tested the mechanical and thermal tool load comparing the turning experiments with the results obtained by FEM simulations. The tools used for the analysis were PcBN inserts with a preparation of the cutting edge carried out in a grinding centre. A 20° chamfer on the rake face was provided to the tool resulting in a negative rake angle of -26°. Referring to the microgeometry, cutting edge rounding was approximated by two chamfers. Different combinations of the cutting segments (S_α and S_γ), symmetrical and asymmetrical, were tested with the values of 20, 30 and 50 µm. The results showed a change in the chamfered of the microgeometry due to the abrasion during the turning process, resulting in a transformation into a continuous rounding of the edge for both experiments, continuous and interrupted cutting. Regarding to the surface quality, the chamfer microgeometry achieved higher surface roughness for continuous and interrupted cutting, comparing to the round cutting edge.

The mechanical tool load was tested with the FEM simulation, and the results showed that a reduction of the internal tool stress occurred with an increase of the length of the cutting segments (S_α and S_γ). This can be explained due to the bigger contact zone between the tool and the workpiece with an increase of the segments, therefore, a more regular distribution of the stresses along the cutting edge was achieved. In addition, a greater influence of S_α was observed. Regarding to the thermal load it was found that, increasing the size of the edge microgeometry, the thermal tool loads are enlarged. As can be seen, the effects of the microgeometry on tool performance are opposite with regard to temperature and stress of the tool. Thus, for achieving the longest tool life, a balance must be reached between thermal and mechanical tool load.

Numerical analyses were carried out by Denkena et al. [DENK12], using AISI 1045 as workpiece material. Different sizes and shapes of microgeometry were tested to study their influence on material flow, process forces and cutting thermal load. 2D FEM simulations were conducted using the software DEFORM 2D V10, 6 µm mesh elements were used around the cutting zone. Heat transfer with the environment was also simulated in order to achieve accurate results of the temperatures generated during the process. Regarding on the material flow, as can be seen in the picture below (Figure 2.9) the size of the stagnation zone increases with the increase of the symmetrical cutting edge rounding (S_α and S_γ). Moreover, the stagnation point increases its height, moving away from the flank face with the increasement of S_α and S_γ.

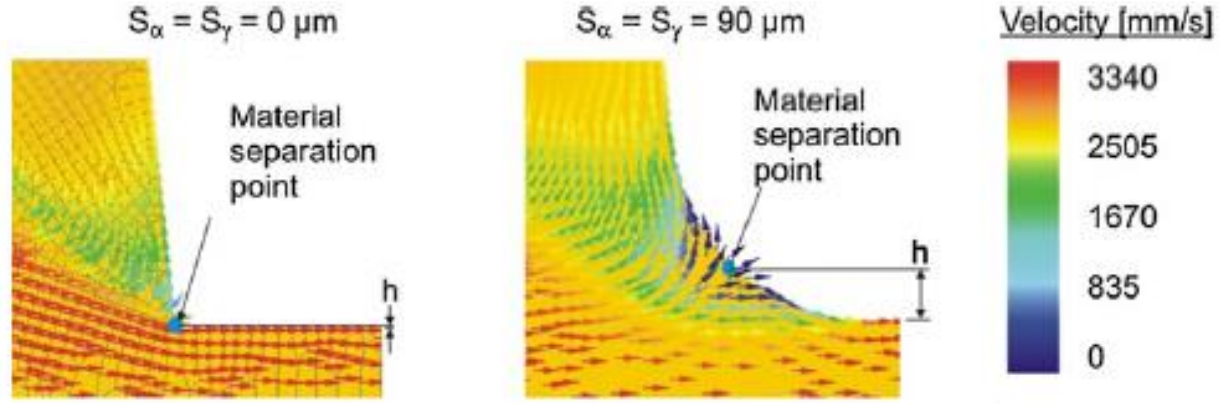

Figure 2.9: Effect of symmetrical rounding on material flow [DENK12]

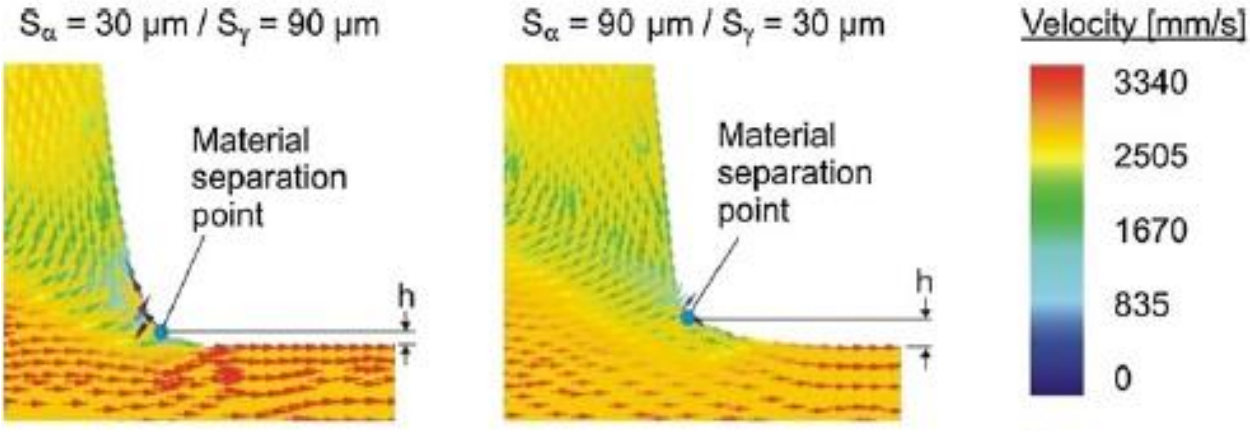

Figure 2.10: Effect of asymmetrical rounding on material flow [DENK12]

On the other hand, Figure 2.10 shows the influence of asymmetrical rounding on the size and shape of the stagnation area. As shown, the influence of the rake face segment (S_γ) is nearly insignificant on the material flow, but it affects the stagnation zone

increasing its size when S_γ increases. S_α has the greatest effect on the size of stagnation zone and height of the material separation point. In addition, the stagnation area created with symmetrical cutting edges is bigger compared to the asymmetrical rounding due to the larger mean cutting edge segment, as can be seen in Figure 2.9 and Figure 2.10.

Regarding to process forces, cutting and feed forces are affected by the microgeometry as it is shown in the FEM simulations. In particular, the cutting force increased with the size of the edge segments. This behaviour can be explained by the lower sharpness of the edge and the distribution of the force over a larger surface. This results in an increasement of the force needed to shear the workpiece material. The feed force, as well as the material flow, is mainly influence by the flank face segment (S_α) while the effect of S_γ is nearly insignificant. S_α is the determining factor for the amount of material that flows under the flank face increasing friction and ploughing effect and as a consequence, increasing feed force.

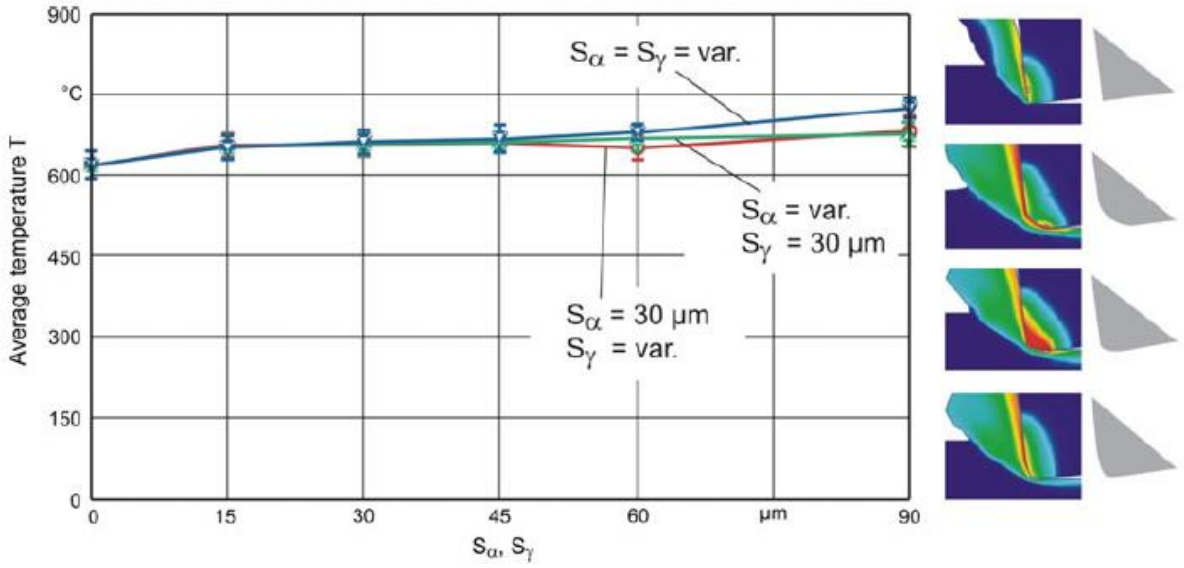

Figure 2.11: Cutting temperature as a function of edge microgeometry. [DENK12]

Concerning the tool thermal load, the cutting temperature rises with an increase of S_α and S_γ due to the more friction and heat generated for the largest microgeometries as can be seen in Figure 2.11. In addition, S_α and S_γ influence the location of the point of the edge with the maximum temperature. For the highest values of S_α, this point is closer to the flank face and increasing S_γ, it shifts to the rake face as shown in Figure 2.12.

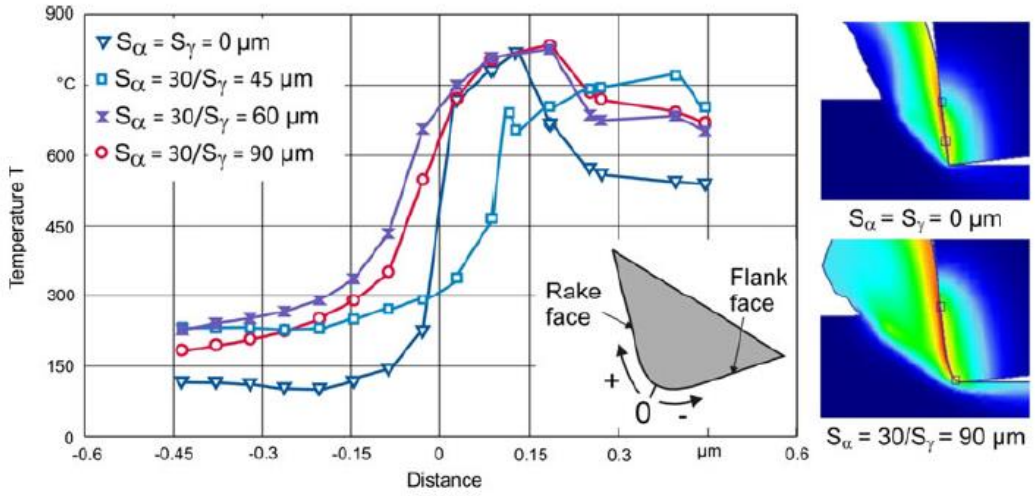

Figure 2.12: Effect of S_γ on rake face and flank face side. [DENK12]

2.5 Chip formation in hard machining

Segmentation of the chip is one of the most important attributes when machining hardened steel with geometrically defined cutting tools. This is a consequence of thermos-plastic instabilities which occur during the cutting process. The crack starts at a point with high compressive stresses, the plastic section of the crack is displaced along the rake face while the chip segment is pushed out, as a result saw-toothed chips are formed [BARR02]. In Figure 2.13 (a) can be seen an example of chip segmentation of a hardened steel with 55 HRC (AISI 52100). Alternatively, the chip obtained when machining steels with lower hardness, saw-toothed chip formation cannot be observed (Figure 2.13 (b)).

Multiple authors have investigated about this topic with experimental and numerical analyses proposing different chip formation mechanisms and damage criteria. Elbestawi et al. [ELBE96] propose a criterion for chip formation and crack propagation based on evaluating surface layer and strain energy density. The fracture problem is considered a mixture of mode I and mode II of crack propagation. Experimental results showed that the fracture angle always was greater than 45° what confirms that the process cannot be completely described by a pure shear problem. For predicting the initial crack angle, surface layer energy was evaluated whereas the angle of fracture propagation can be calculated using strain energy density. Hard turning tests were carried out with AISI 1550 hardened steel as the workpiece. The experimental results confirmed the prediction calculated using the analytic equations proposed by the author based on fracture mechanics and strain energy.

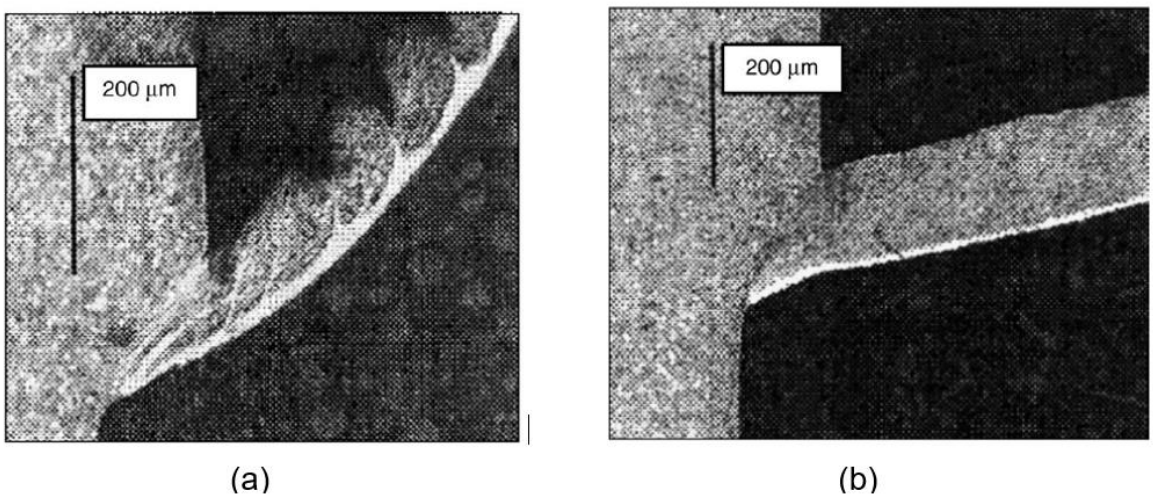

Figure 2.13: Morphology of the chip [UMBR04]. (a) steel with 55 HRC. (b) steel with 40 HRC

The improvement in finite elements techniques and the increase in the calculation capacity of computers allowed the development of new theories about chip formation. Most recent studies use Johnson-Cook stress model and Brozzo damage criteria or a modification derived from them. Tiffe et al. [TIFF19] performed analyses using a modified Johnson-Cook model that consider the grain boundary sliding (GBS) into the flow model. The experiments and simulations performed using 51CrV4+Q hardened steel as the workpiece material. Numerical results predicted chip segmentation showed in Figure 2.14 and it is compared with the chip cross section obtained in the experimental tests. The results of the simulations matched with the experiments for both low and high cutting speeds (12 and 180 m/min) in contrast with conventional flow stress models which cannot predict accurately the chip formation for low cutting speeds.

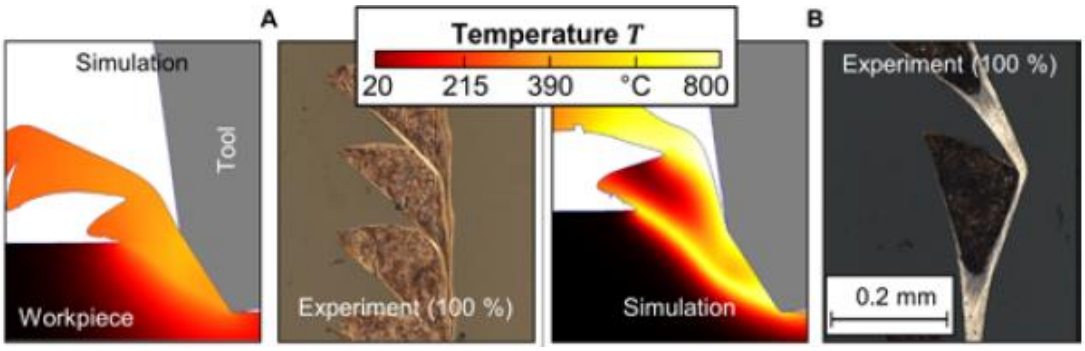

Figure 2.14: Comparison of the results achieved with simulations and experiments of chip formation for low (left) and high (right) cutting speed. [TIFF19]

Umbrello et al. [UMBR04] developed a hardness-based flow stress model considering a non-isothermal viscoplastic material. Numerical simulations were performed using hardened steel AISI 52100 and comparing them with experimental results of the literature to validate the model. Mainly, the morphology of the chip depends on the hardness of the material and the cutting speed. Therefore, two different scenarios were tested, one with a workpiece with an initial hardness of 41 HRC and other with 55 HRC. For the harder workpiece segmentation of the chip was observed, on the other hand, the softer one obtained a continuous chip (Figure 2.15). Comparing these results with experiments carried out in the literature, the author conclude that the method can predict precisely orthogonal cutting processes.

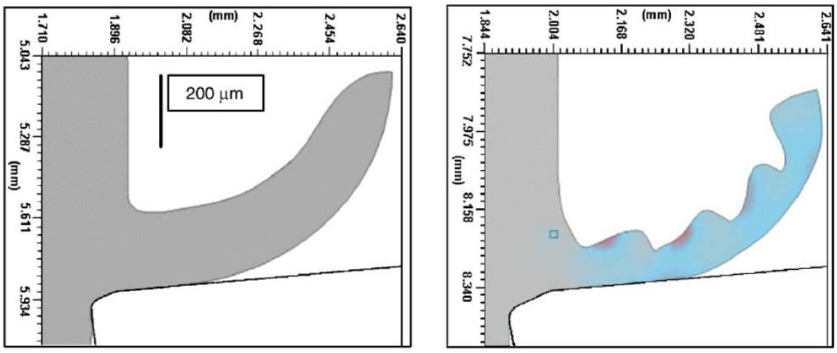

Figure 2.15: Chip formation simulations of steels with 41 HRC (left) and 55 HRC (right). [UMBR04]

3 Research approach

The machining of hardened steels presents a challenge due to high thermomechanical tool load that appears during the process, polycrystalline cubic boron nitride tools (PcBN) are commonly used. Due to the directly contact between the tool and the workpiece during the cutting process when using geometrically defined cutting edges, the size and shape of it influence genuinely tool behaviour as well cutting forces and chip formation. The focus of this thesis is to analyse the influence of cutting edge microgeometry on surface quality, process forces and chip formation when machining AISI 52100 bearing steel. The exact relations between them are currently unknown.

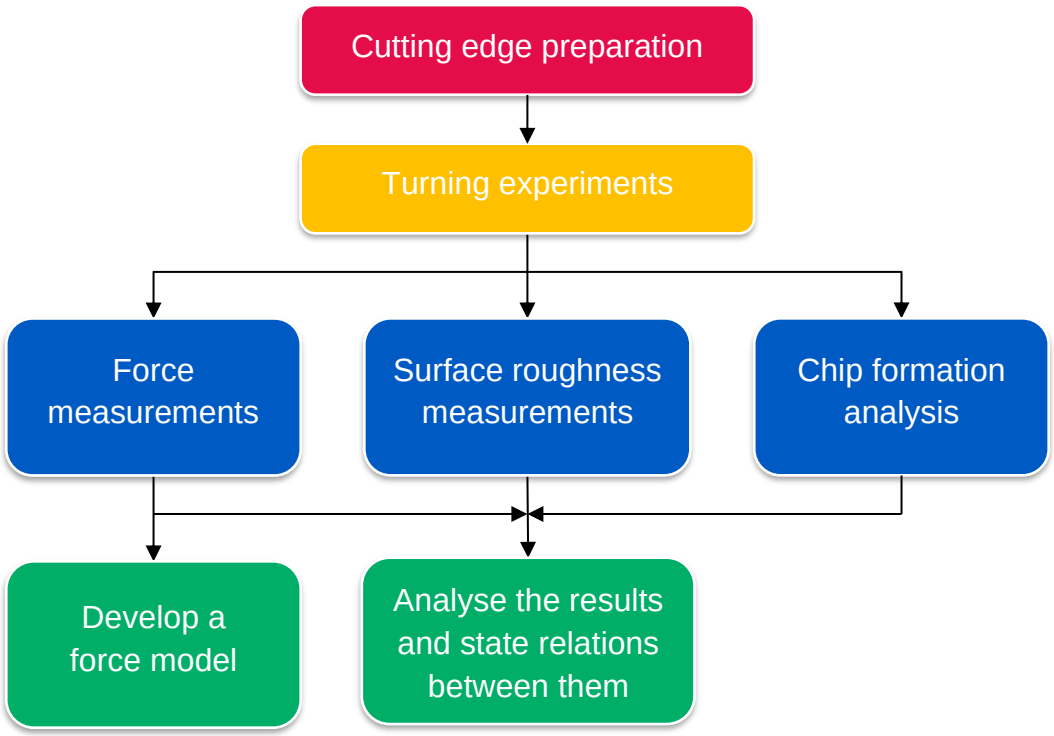

Figure 3.1: Research approach

Figure 3.1 shows the research approach followed along this thesis, the first step was the cutting edge preparation using two different methods, brushing and grinding. Following, for the turning experiments, different microgeometries were tested using different cutting parameters. During the process, the cutting forces were monitored and later postprocessed. Using the measured values, a force model was developed in order to predict the cutting forces as a function of the engagement area, which depends on the feed rate and cutting depth. In addition, the roughness of the machined surface was measured, and the chips section were analysed under the microscope. Finally, an in-depth analysis was carried out to state relation between all the results.

4 Experimental set-up

4.1 Workpiece material

The material used as the workpiece in all tuning experiments was AISI 52100 hardened steel with high carbon content. It can be also named with the designation 100Cr6 in Europe. This material is commonly used for manufacturing bearings due to its mechanical properties, such as high hardness and high wear resistance. The chemical composition and physical properties of the workpiece material can be seen in Table 2 and Table 3 respectively.

Table 2: Composition of AISI 52100 [ZHAO17]

C	Mn	Si	Cr	Ni	Mo	Cu	S
0.9-1.05	0.25–0.45	0.15–0.35	1.35–1.65	<0.3	-	0.3	<0.025

Table 3: Physical properties of AISI 52100 [UMBR04]

	Density (kg/m^3)	Young's modulus (GPa)	Poisson's ratio	Thermal conductivity (W/mK)	Coefficient of thermal expansion (10^{-6} /K)	Specific heat capacity (J/kgK)
20 °C	7853	210	0.3	54	1.2	510
500 °C				39		740
1000 °C				31		550

4.2 Turning operations

The turning tests were carried out in a Hembrug Mikroturn 100 CNC lathe. The tools used were CNMA120408 PcBN inserts. The workpiece was a cylindrical part with a diameter of 160 mm made of AISI 52100. About cutting forces measurement, a Kistler type 9121 3-axis dynamometer was use for this task, cutting, feed and passive forces were measured and then postprocessed to achieve their final values.

Regarding to signal processing, Kistler type 5011 charge amplifiers were employed, one per force channel. The signal was converted analog to digital for sending the data to the measuring software. With the force measurement completed, the results were analysed using Matlab and applying a low-pass filter for dismiss the higher frequencies produced by tool vibrations.

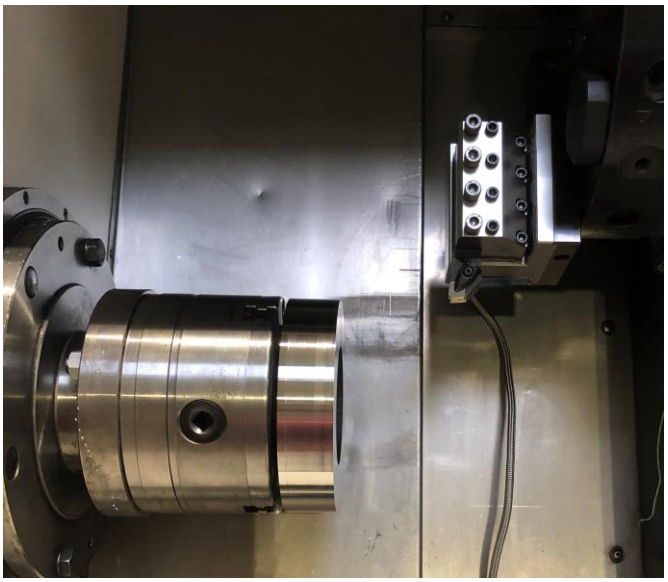

Figure 4.1: Turning set up and workpiece. Force dynamometer, tool holder and PcBN insert.

4.3 Cutting edge preparation

In order to stabilize the cutting edge, a precise adjustment of the tool microgeometry has shown to be useful. Consequently, numerous techniques have been developed during the last decades for cutting edge preparation. Some examples of it are brushing, grinding, abrasive jet machining or laser machining. Different processes obtain different results regarding to performance and obtained edge microgeometries. For the turning tests, different tools have been prepared using grinding and brushing methods, achieving symmetric and asymmetric microgeometries.

4.3.1 Brushing

Brushing is a machining process with a geometrical undefined cutting edge. A disk brush is used for the material removal. It is composed of filaments commonly made of nylon and an abrasive material such as SiC (silicon carbide) or PCD (polycrystalline diamond). The tool is fixed to a 5-axis machine which can achieve the desired geometry for rounded cutting edges. The microgeometry obtained is a consequence of multiple factors, such as, cutting speed, infeed, setting angle and brushing time because the material removal of the cutting edge increases. The size of the microgeometry is highly influence by the brushing time and the infeed. On the other hand, the shape of the microgeometry is affected by the setting angle, being the most important factor to

achieve symmetrical or asymmetrical cutting edges. With brushing techniques, a continuous rounding can be achieved.

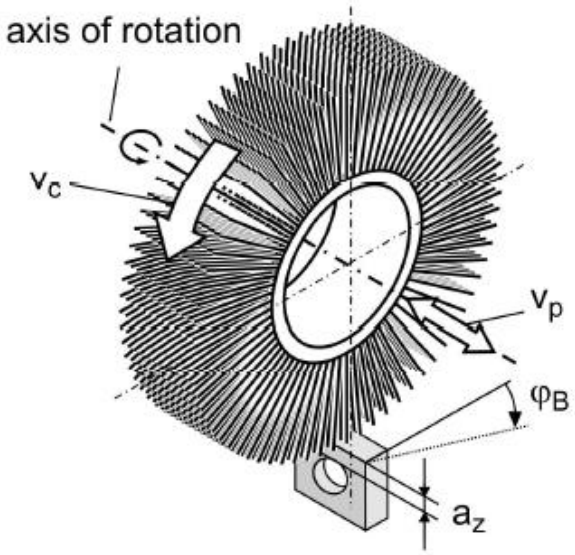

v_c = cutting speed

a_z = infeed

V_p = oscillation speed

φ_B = setting angle

Figure 4.2: Brushing processes. [DENK10]

For the experiments, the PcBN inserts were brushed using an industrial robotic arm which allows a complete control of all the process parameters in order to achieve the desired microgeometries. The disk brush is made of nylon filaments and diamond grains as the abrasive material. Figure 4.3 shows the robotic arm used and the tool holder for the PcBN insert. Figure 4.4 shows the disk brush used for the process.

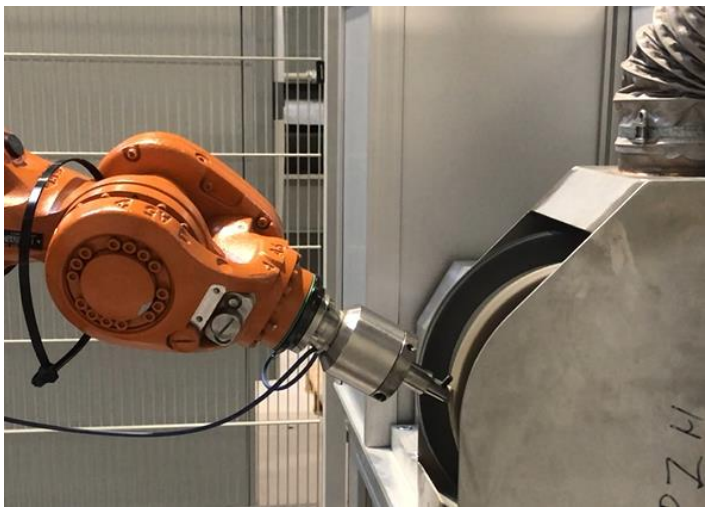

Figure 4.3: Robotic arm used for brushing.

Figure 4.4: Disk brush used for brushing.

The tools were provided with a sharp cutting edge and with a chamfer on the rake face. The chamfer angle is $y_f = 20°$ with a width of $b_f = 150$ µm. Four different tools were prepared with brushing techniques, two symmetrical and two asymmetrical microgeometries as can be seen in Table 4.

Table 4: Brushed tools

Tool No.	**1B**	**2B**	**3B**	**4B**
$\mathbf{S_\alpha}$	15	30	50	50
$\mathbf{S_\gamma}$	15	50	30	50

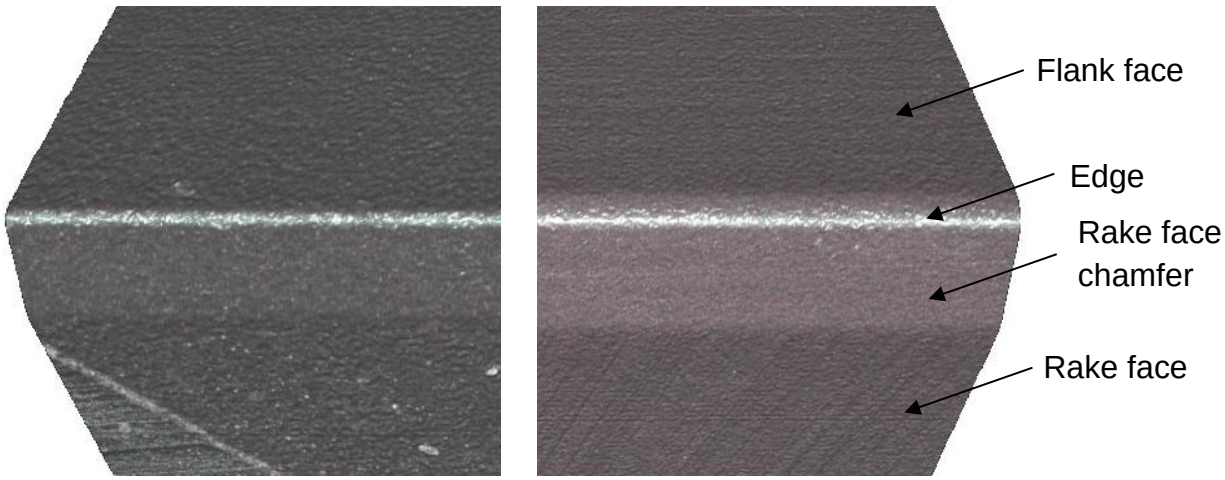

Figure 4.5: Brushed edge with symmetrical microgeometry of tools 1B (S_α/S_γ = 15/15 µm) (left) and 4B (S_α/S_γ = 50/50 µm) (right)

Figure 4.5 shows the symmetrical edges of tools 1G and 4G produced with brushing. The microgeometry achieved has a continuous rounding, which is typical of brushing. Normally, PcBN tools for hardened steel incorporate a rake face chamfer, as can be seen in the picture below.

4.3.2 Grinding

Grinding is a type of abrasive machining with an undefined cutting edge. A grinding wheel is used in the process for material removal. Grinding preparation is commonly carried out in 5-axis grinding centres which allow to achieve precise edge microgeometries. With grinding processes, continuous rounding cannot be achieved, therefore, it can be approximated by multiple chamfers as seen in Figure 4.6.

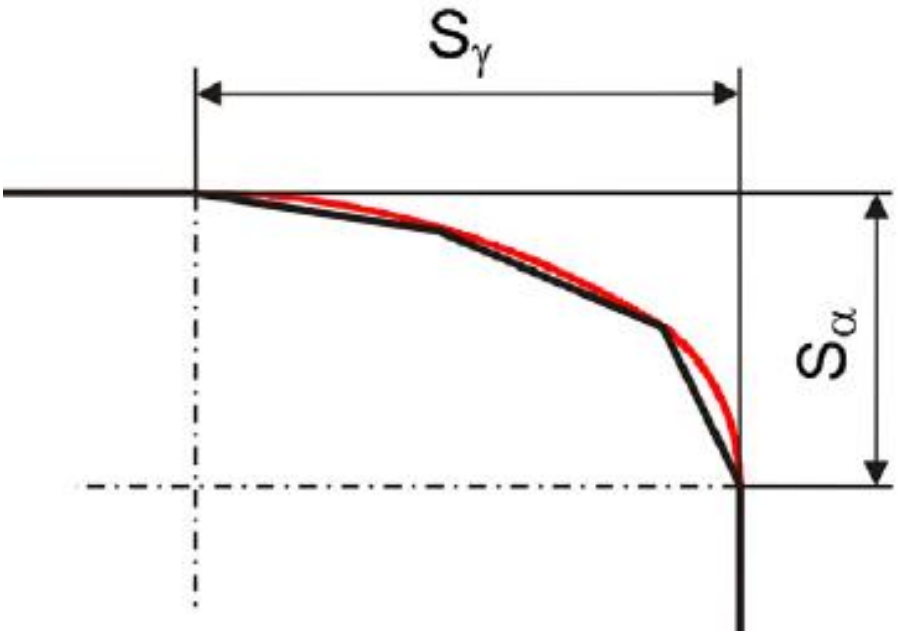

Figure 4.6: Continuous rounding approximated by multiple chamfers. [VENT13]

For PcBN cutting tools, grinding wheels with smaller diamond grains achieve better edge quality because the single grain chip thickness is reduced, being the dominant parameter in the grinding process. Regarding to feed velocities, lower speeds can achieve better edge quality with a reduction in productivity. The same occur with high cutting speeds, they can cause edge damage as a consequence of the high temperatures reached. [VENT13]

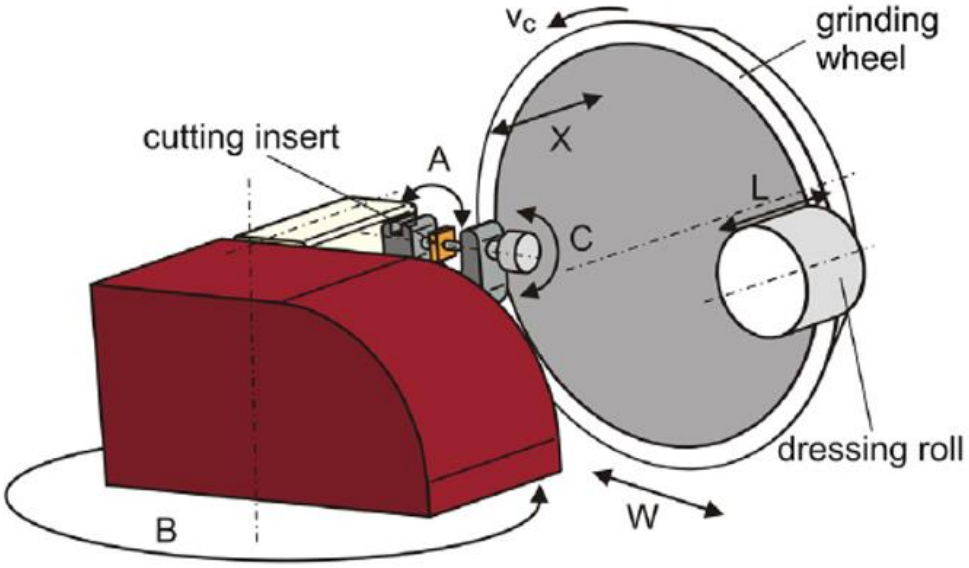

Figure 4.7: 5-axis grinding centre. [DENK13]

The tools used in the experiments were prepared in a 5-axis grinding centre Wendt WAC 715 Centro (Figure 4.7). A diamond grinding wheel with a grain size of 10 µm was used for the edge preparation. As well as for the brushed tools, the ground tools were provided with a sharp cutting edge and with a chamfer on the rake face. The chamfer angle is $\gamma_f = 20°$ with a width of $b_f = 150$ µm. On the other hand, a chamfer on the flank face was ground with an allowance of 0.05 mm. The process parameters are detailed in the following table (Table 5).

Table 5: Grinding parameters

Cutting speed (m/s)	Feed rate (mm/min)	Radius velocity (°/min)	Dressing feed (m/s)
30	6	2887	0.1

Four different tools were prepared with grinding techniques, two symmetrical and two asymmetrical microgeometries with different values of S_α and S_γ as can be seen in table below (Table 6).

Table 6: Grounded tools

Tool No.	1G	2G	3G	4G
S_α	30	30	50	50
S_γ	30	50	30	50

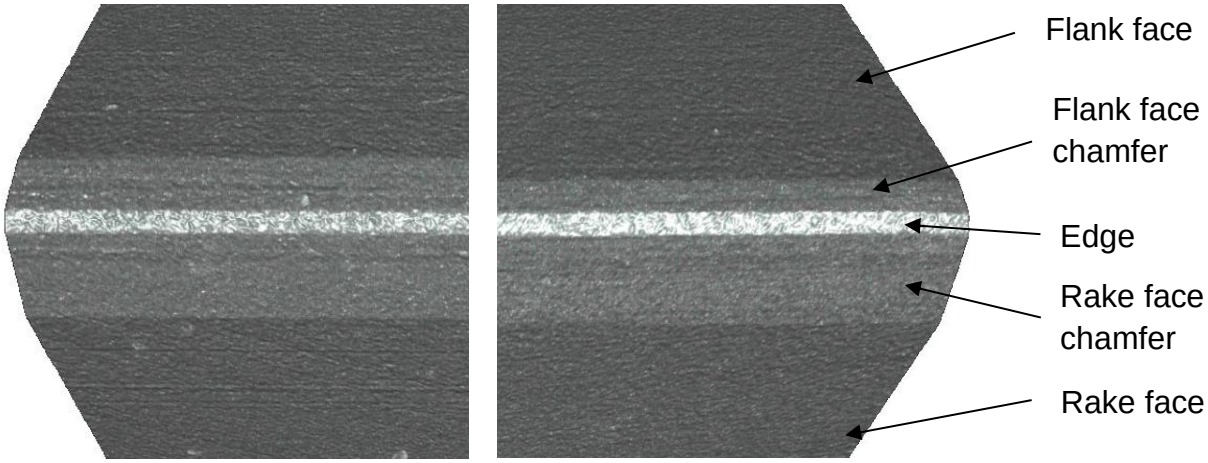

Figure 4.8: Ground edge with asymmetrical microgeometry of tools 2G (S_α/S_γ = 30/50 µm) (left) and 3G (S_α/S_γ = 50/30 µm) (right)

In Figure 4.8 is shown two ground edge microgeometries. An approximation of a rounded edge is used in this tool due to the limitations of the preparation technology used. Two chamfers can be seen in the picture, one on the rake face and other on the flank face. The first is commonly used for hard machining with PcBN tools, and the second was machined at the grinding centre at the same time as the microchamfers, during the cutting edge preparation.

5 Analysis of the process forces

For the turning experiments carried out in the Mikroturn CNC lathe, different cutting parameters were tested in order to study their influence on the cutting forces. During the tests, the cutting, feed and passive forces were monitored in order to analyse the influence of the cutting parameters in the process forces. On the other hand, a force model was developed using two different methods (maximum uncut chip thinness and engagement area) with the aim of predict the cutting forces as a function of the process parameters. Along this chapter only the symmetrical edges were used during the experiments.

5.1 Analysis of the process forces depending on the process parameters

With the purpose of analyse the influence of the process parameters (cutting speed, feed rate and cutting depth) in the process forces for different microgeometries, numerous turning experiments were carried out. The first analysis was performed varying the cutting speed as shown in Table 7. The two symmetrical tools were used for these investigations, tools with the edge microgeometry of S_α/S_γ = 30/30 and S_α/S_γ = 50/50.

Table 7: Cutting parameters for different cutting speed

Cutting conditions No.	**1**	**2**	**3**	**4**	**5**	**6**	**7**
Cutting speed (m/min)	50	75	100	130	160	180	200
Feed rate (mm/rev)	0.1	0.1	0.1	0.1	0.1	0.1	0.1
Depth of cut (mm)	0.2	0.2	0.2	0.2	0.2	0.2	0.2

In Figure 5.1 can be seen the influence of the cutting speed in the tangential force (cutting force F_c). The results reported a decreasing tendency of the force when increase the cutting speed. This behaviour agrees with the studies carried out by some authors of the literature [BOUA10] and can be explained due to the thermal softening as a consequence of the increase of relative velocity between the tool and the workpiece. The temperature of the area around the edge rises for the higher cutting speeds. Therefore, the force needed to shear the material decreases. On the other hand, the largest microgeometry needs higher forces as has been described in previous chapters. In the figure below can be seen some values that differ from linear regression, it can be attributed to experimental errors or signal noise due to the experimental procedure.

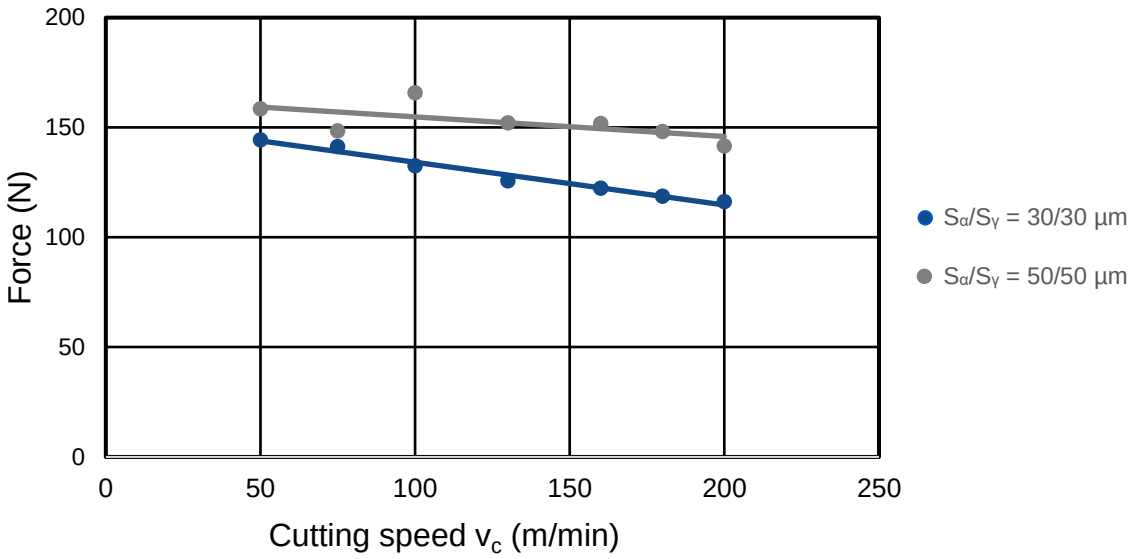

Figure 5.1: Cutting force as a function of cutting speed.

Figure 5.2 shows the feed force as a function of the cutting speed. As for the cutting force, for the highest cutting speeds, the feed force decreased due to the increasing of cutting temperature for both microgeometries.

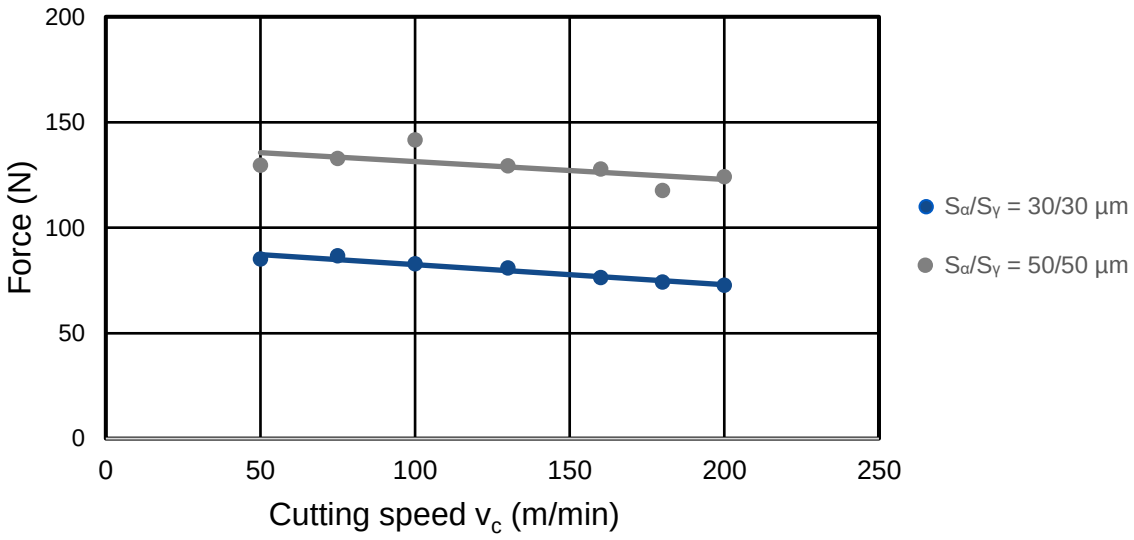

Figure 5.2: Feed force as a function of cutting speed.

In Figure 5.3 can be seen the influence of cutting speed in passive force. A slightly decrease has been found with increasing cutting speed. The passive component is the less affected force by the cutting speed. Some values deviate from the linear regression, as can be seen in the figure below. It is assumed that these deviations come from errors in experimental procedure.

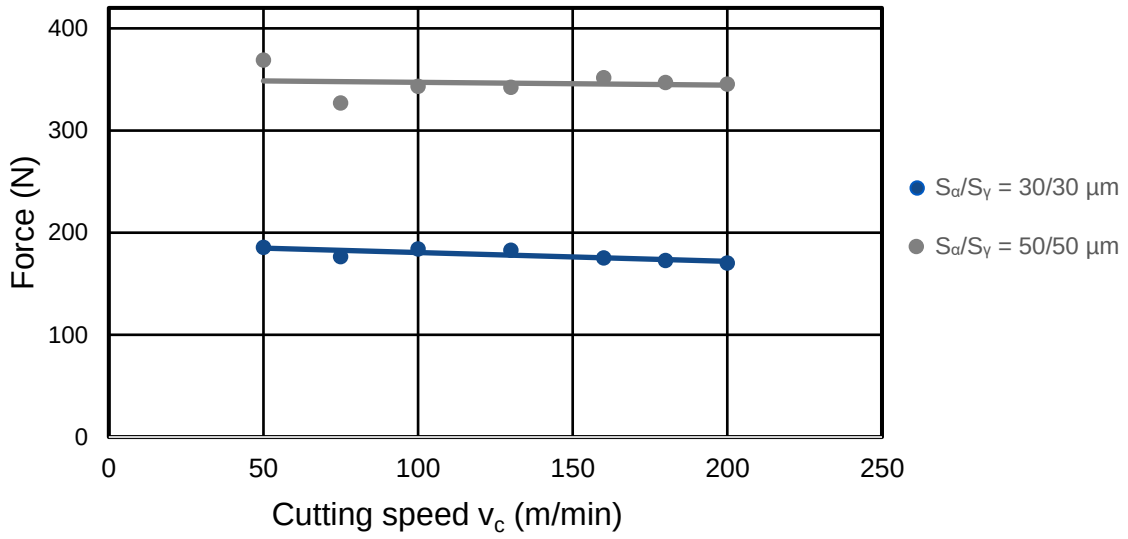

Figure 5.3: Passive force as a function of the cutting speed.

Regarding to the influence of cutting depth, continuous cutting experiments were carried out using different depths of cut, in order to investigate the effect of it in the process forces. For these tests, only the symmetrical tools were used, tool with microgeometry of S_α/S_γ = 30/30 µm and tool 4G (S_α/S_γ = 50/50 µm). The cutting speed and feed rate were 160 m/min and 0.1 mm/rev respectively. The cutting depth was adjusted to the following values: 0.05, 0.1, 0.2 and 0.3 mm.

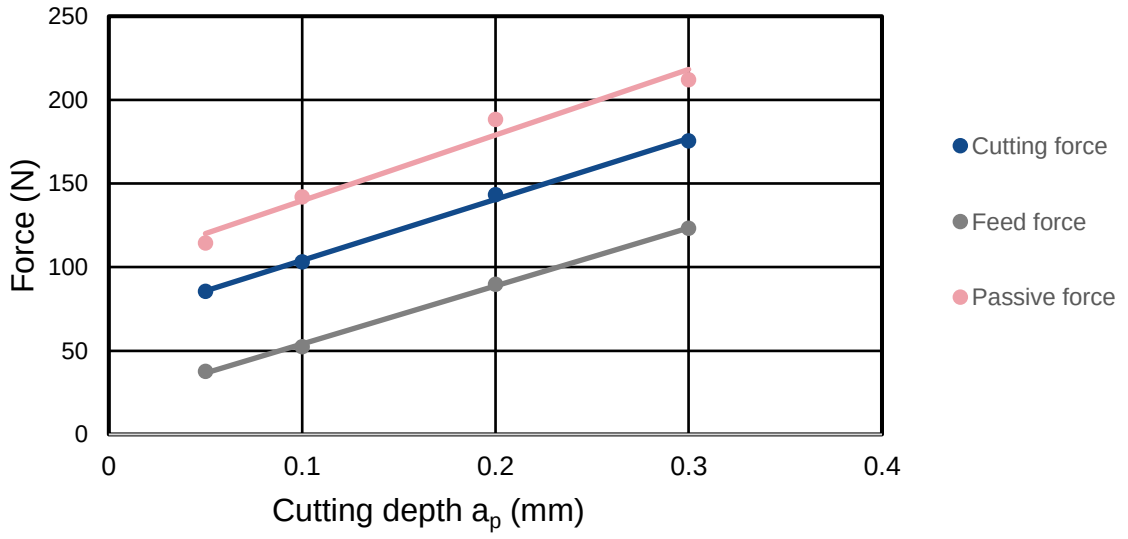

Figure 5.4: Process forces as a function of cutting depth. S_α/S_γ = 30/50 µm

In Figure 5.4 can be seen the process forces as a function of the cutting depth for tool with microgeometry of S_α/S_γ = 30/30 µm. The results showed a linear dependency of

the forces with respect to the depth of cut. For all the different values of cutting depth, the passive force reached the higher values while the feed force took the lower values, as is expected in hard turning.

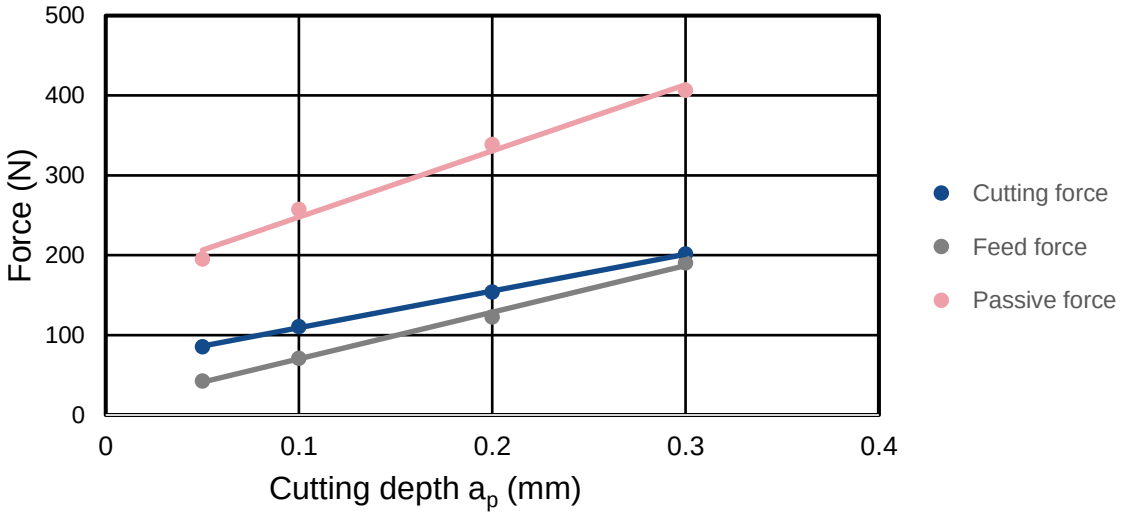

Figure 5.5: Process forces as a function of cutting depth. S_α/S_γ = 50/50 µm

The results obtained using tool tool with microgeometry of S_α/S_γ = 50/50 µm are shown in Figure 5.5. As well as for the tool 1G, the values of the forces for the different cutting depths approximate to a line, showing a linear dependency.

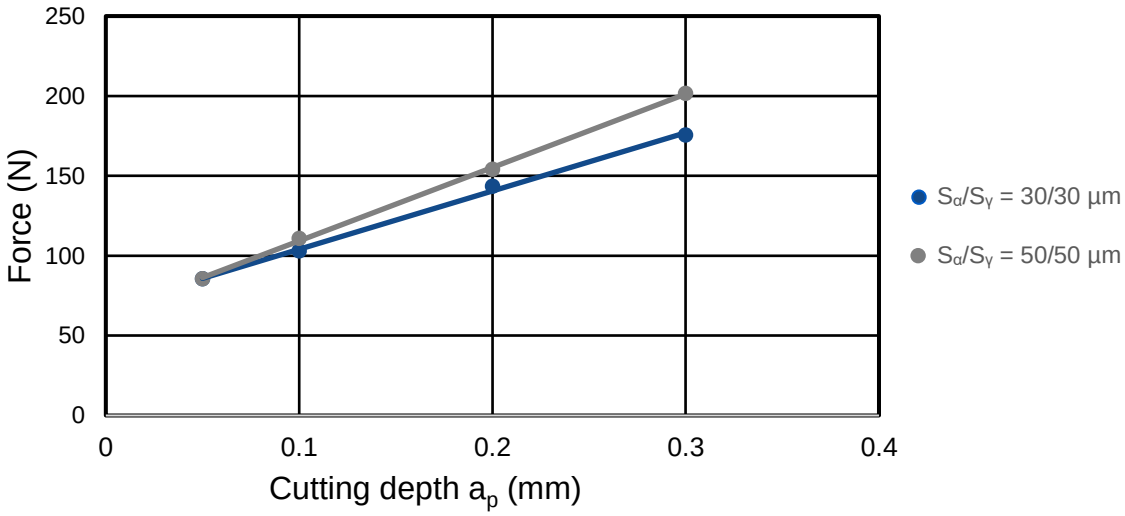

Figure 5.6: Cutting force as a function of cutting depth.

Figure 5.6 shows the comparison of the cutting force between tool 1G and 4G. The linear dependency of the cutting force can be seen in the figure for both edge

microgeometries. As has been previously commented, the edges with bigger microgeometries need higher forces to shear the workpiece material. However, the slope of the line described by the values of the force, is higher for the biggest microgeometry. Therefore, the same increase in cutting depth will produce a larger increasement in the force for the 50/50 edge.

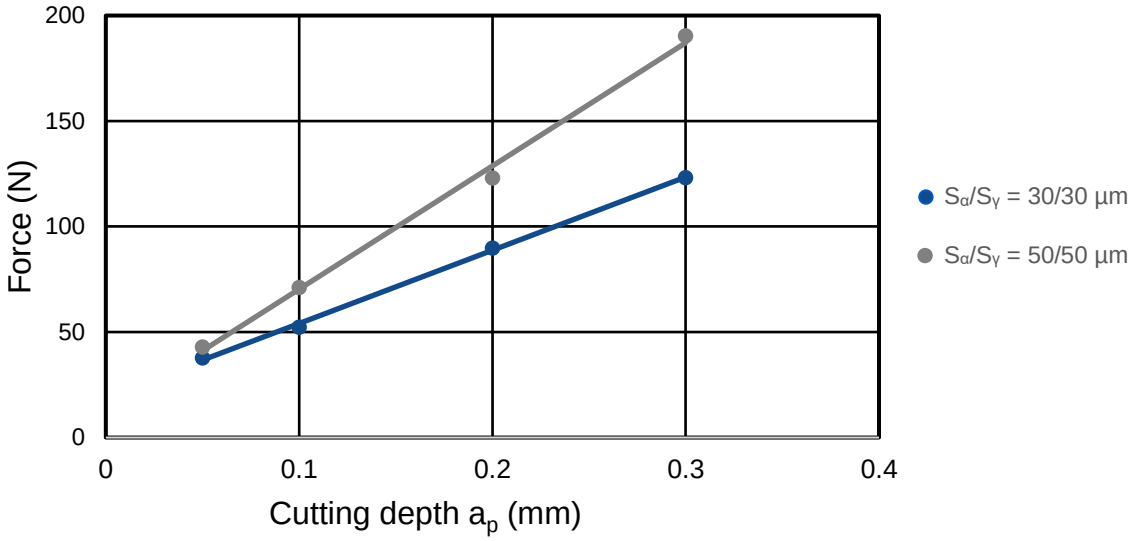

Figure 5.7: Feed force as a function of cutting depth.

Figure 5.7 shows the comparation between feed force for the tool 1G and 4G. The feed force is higher for the S_α/S_γ = 50/50 µm geometry, and the slope of the linear regression is higher as shown in the figure.

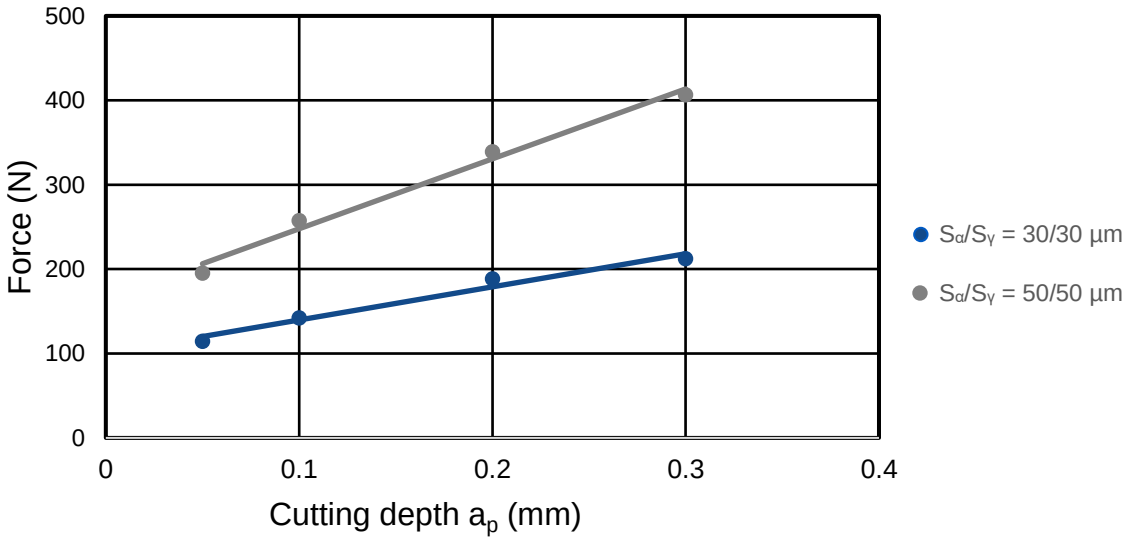

Figure 5.8: Passive force as a function of cutting depth.

Figure 5.8 shows the variation of passive forces for both tools. As has been previously mentioned, the passive force is the dominant when hard turning. The results revealed a higher variation for the largest microgeometry as well as for cutting and feed force. In the other cases, the values of the forces for small cutting depth were similar, in contrast with passive force, which exist a much bigger force for the lowest cutting depth.

Finally, in order to investigate the influence of the feed rate in the forces involved in turning processes, different tests were conducted using different values of it. As expected with increasing feed rate, all the process forces will increase because of the tool is shearing more material per each revolution. The cutting parameters are described in Table 8.

Table 8: Cutting parameters for different feed rates

Cutting conditions No.	**1**	**2**	**3**	**4**
Feed rate (mm/rev)	0.05	0.1	0.2	0.3
Cutting speed (m/min)	160	160	160	160
Depth of cut (mm)	0.2	0.2	0.2	0.2

The cutting force is genuinely influenced by the feed rate, as commented before, cutting force increases with the increasing feed rate. Figure 5.9 shows the cutting force as a function of the feed rate for the symmetrical edges, the tools with the geometry S_α/S_γ = 30/30 µm and S_α/S_γ = 50/50 µm, the largest microgeometry reported the higher forces.

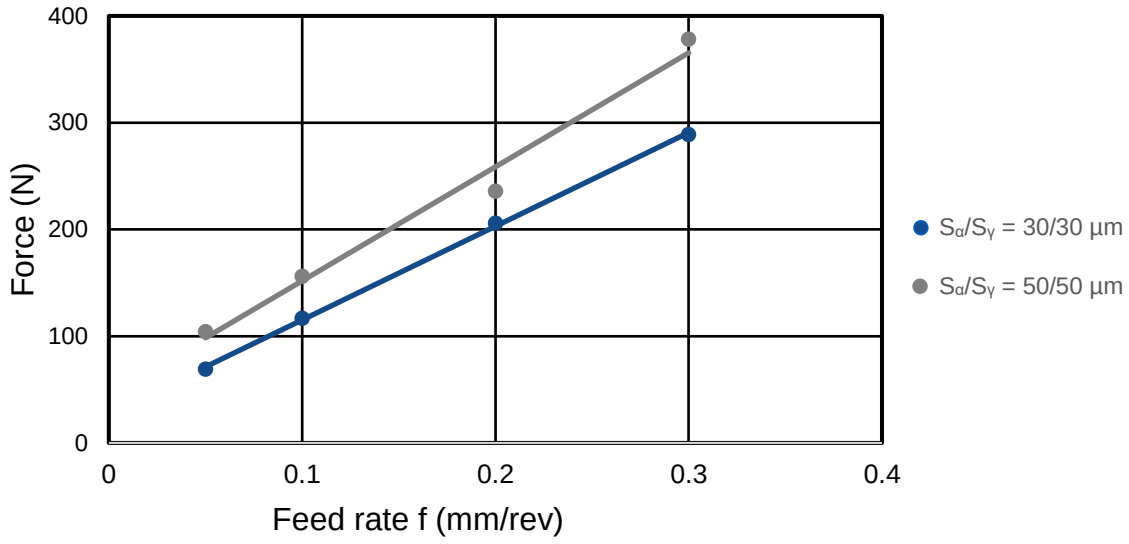

Figure 5.9: Cutting force as a function of feed rate.

Figure 5.10 shows the values of the feed force with the variation of feed rate. As expected, a raise of feed rate causes an increase of feed force for both microgeometries. Note that the slope of the values for both geometries is similar.

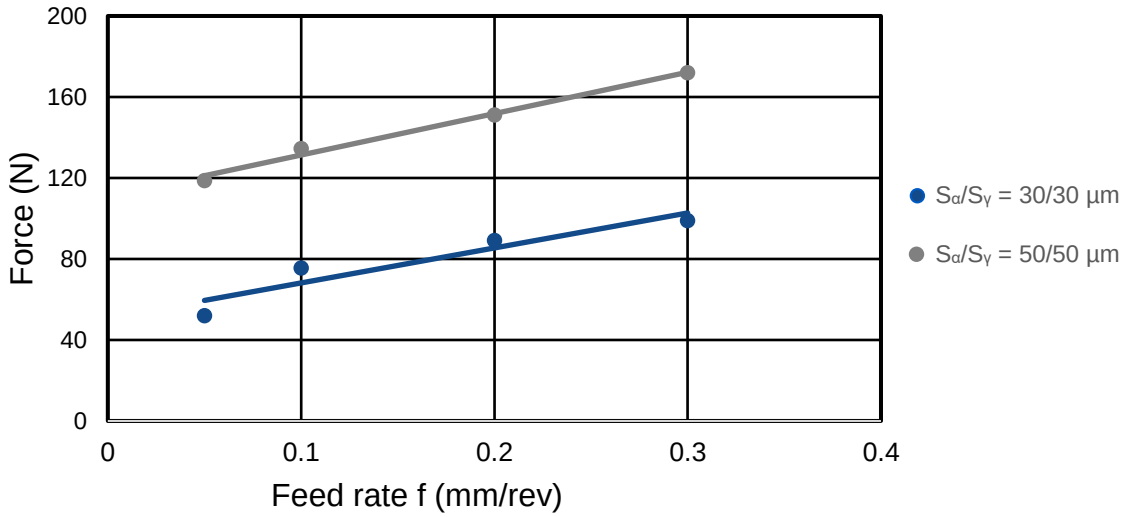

Figure 5.10: Feed force as a function of feed rate.

Finally, Figure 5.11 shows the passive force measured on the turning tests as a function of the feed rate. As described for the previous cases, the force increases when increasing the feed rate. In the figure below can be observed the line created by the measured points has a greater slope for the biggest microgeometry as occurs when varying the cutting depth.

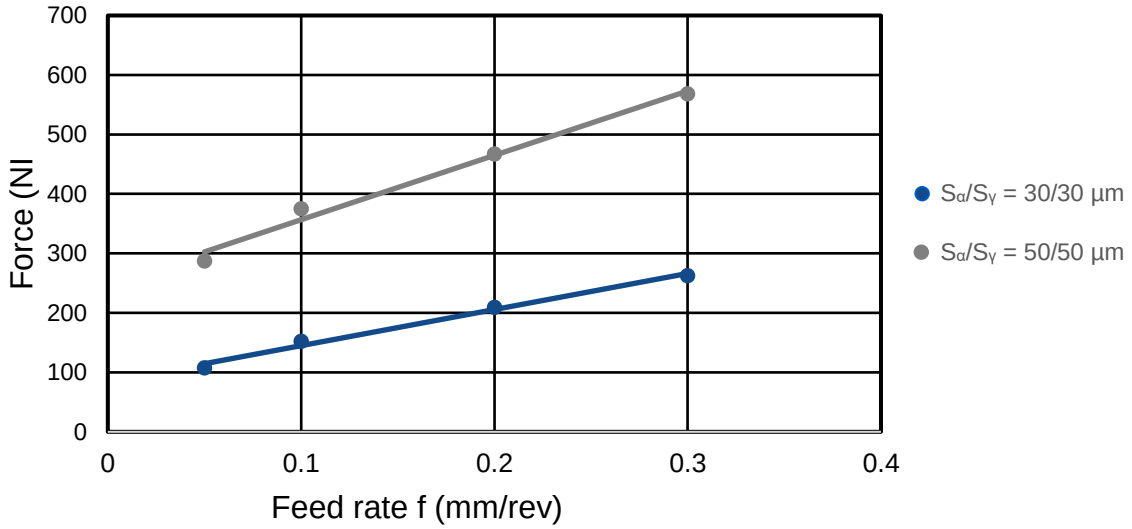

Figure 5.11: Passive force as a function of feed rate.

5.2 Development of a force model for hard turning

In the previous chapter, a linear correlation between f and ap with regard to the process forces was found. But there are interactions between f and ap that were not taken into account. Therefore, a force model has been developed in order to predict the process forces as a function of the cutting parameters. The measured values of the forces have been evaluated as a function of the maximum uncut chip thickness (h_{max}) and the engagement area (A_e) obtaining different results for both approximations. In the first place, model using the engagement area has been calculated. Figure 5.12 shows the engagement area which can be evaluated as a function of the feed rate (f), cutting depth (a_p) and nose radius of the tool (R_ε) as shown in the figure. O_1 and O_2 are the centres of the nose rounding of the tools. The area is the enclosed region between two circumference segments with radius the nose radius of the tool insert, separated by the value of the feed rate and the heigh corresponding to the depth of cut. Note that the engagement area has a linear dependency with the depth of cut and the feed rate and in previous chapters has been shown a linear relation between process forces and cutting parameters. Therefore, it can be expected that there will be a linear relation between the engagement area and the process forces.

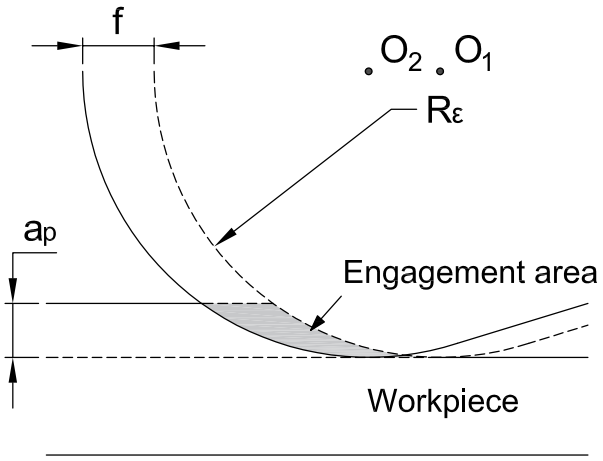

Figure 5.12: Engagement area

Figure 5.13 and Figure 5.14 shows the linear dependency of the cutting forces with the engagement area of the tool 1G and tool 4G with the microgeometry S_α/S_γ = 30/30 µm and S_α/S_γ = 50/50 µm respectively. A force model has been fitted to the measured values obtaining the equation *5.1*.

$$F = M \cdot A_e + N \qquad (5.1)$$

Being F the process force, A_e the engagement area and M and N two constants described in Table 9. Regarding to the units, M is expressed in N/mm^2 and N in newtons while F is expressed in newtons and A_e in mm^2.

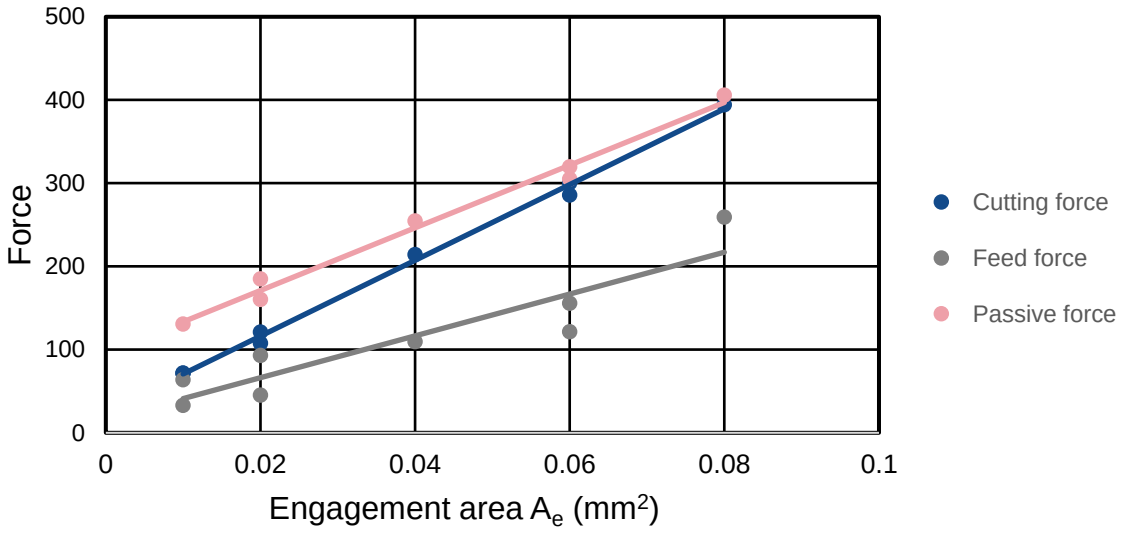

Figure 5.13: Process forces as a function of the engagement area. S_α/S_γ = 30/30 µm, v_c=160 m/min

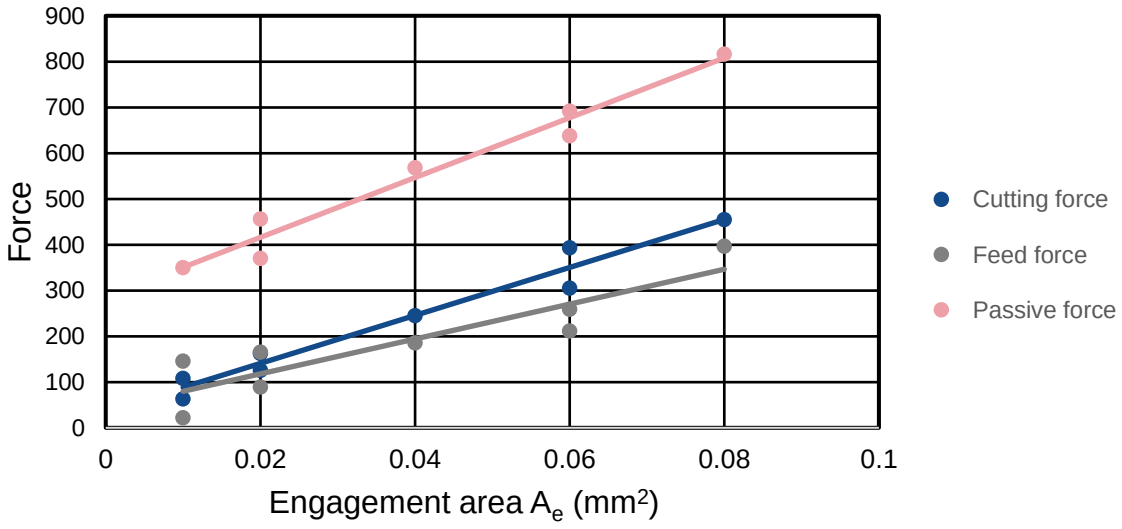

Figure 5.14: Process forces as a function of the engagement area. S_α/S_γ = 50/50 µm, v_c = 160 m/min

Table 9 shows the values of the constants for the force model based on the engagement area. Additionally, the table shows the values of R-squared, which evaluates the quality of the linear regression, and as can be seen in the table, for cutting and passive

forces the value reaches 0.96 which means an accurate approximation of the model to the real values. In contrast the feed force reported lower values of R^2 of around 0.84.

Table 9: Constants for the engagement area force model

	Cutting Force		Feed Force		Passive force	
	S_α/S_γ = 30/30 µm	S_α/S_γ = 50/50 µm	S_α/S_γ = 30/30 µm	S_α/S_γ = 50/50 µm	S_α/S_γ = 30/30 µm	S_α/S_γ = 50/50 µm
M	4552.3	5238.9	2513.2	3808.8	3766	6533.3
N	25.15	35.9	15.9	41.6	95.69	285.2
R^2	0.9967	0.9604	0.8455	0.8033	0.9872	0.9668

The second force model was developed based on the maximum uncut chip thickness (h_{max}) according to Eqs. 5.2 and 5.3. It has been calculated as a function of the feed rate (f), cutting depth (a_p) and nose radius of the tool (r_ε).

$$\kappa_{eff} = \frac{1}{2} \cdot arccos\left(\frac{r_\varepsilon - a_p}{r_\varepsilon}\right) \quad (5.2)$$

$$h_{max} = f \cdot sin\,(2 \cdot \kappa_{eff}) \quad (5.3)$$

Figure 5.15 and Figure 5.16 show the linear dependency of the cutting forces with the maximum uncut chip thickness of the tools with the microgeometry S_α/S_γ = 30/30 µm and S_α/S_γ = 30/30 µm. A force model has been fitted to the measured values, as well as for the previous model, a linear regression was applied obtaining the equation *5.1*.

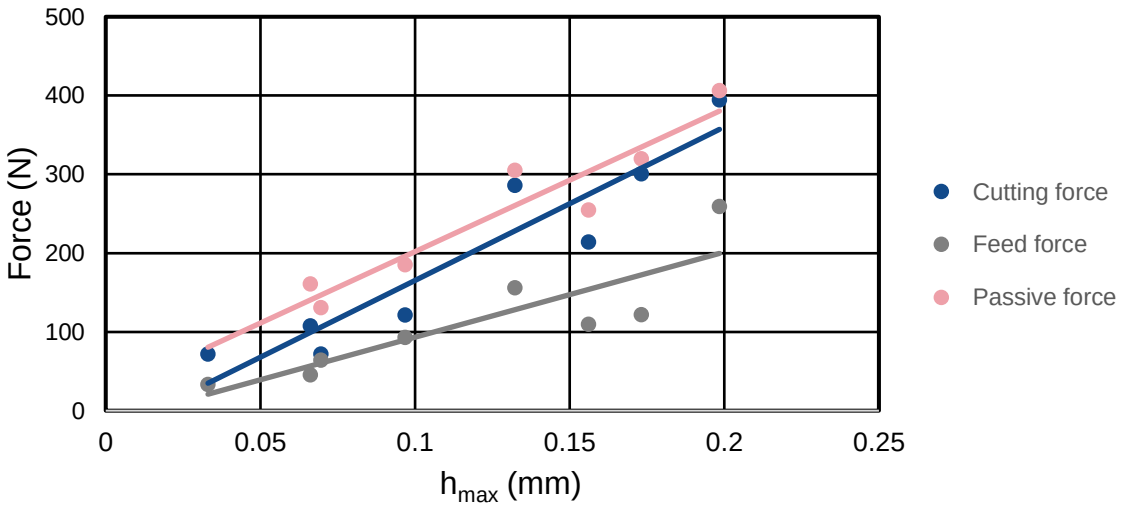

Figure 5.15: Process forces as a function of the maximum uncut chip thickness. S_α/S_γ = 30/30 µm, v_c=160 m/min

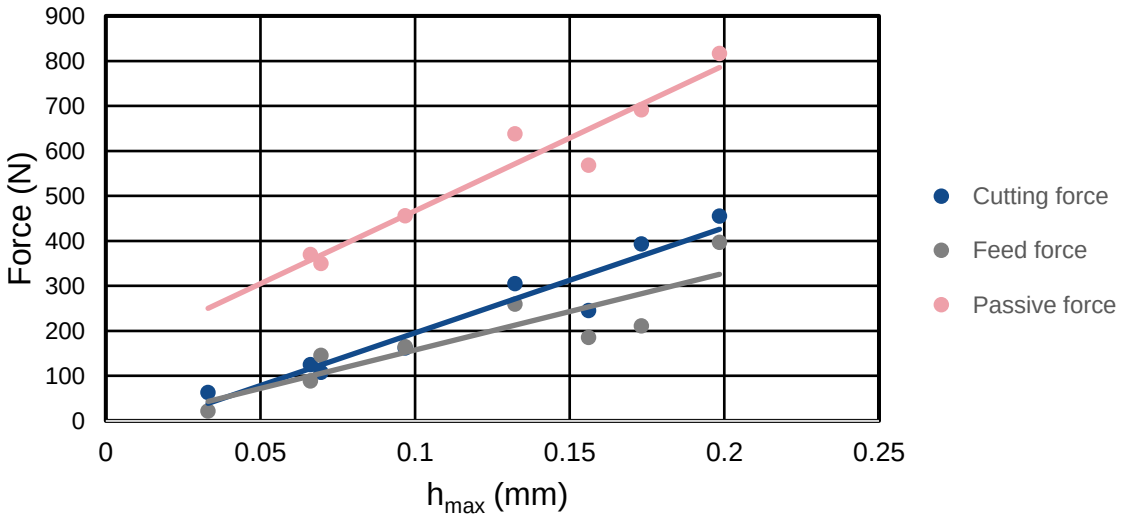

Figure 5.16: Process forces as a function of the maximum uncut chip thickness. S_α/S_γ = 50/50 µm, v_c=160 m/min

Table 10: Constants for the h_{max} force model

	Cutting Force		Feed Force		Passive force	
	S_α/S_γ = 30/30 µm	**S_α/S_γ = 50/50 µm**	**S_α/S_γ = 30/30 µm**	**S_α/S_γ = 50/50 µm**	**S_α/S_γ = 30/30 µm**	**S_α/S_γ = 50/50 µm**
M	1948.6	2340.2	1080.9	1708.8	1813	3236.8
N	-29.62	-38.424	-14.883	-13.29	20.53	143.12
R^2	0.8791	0.9224	0.7528	0.7832	0.8971	0.9304

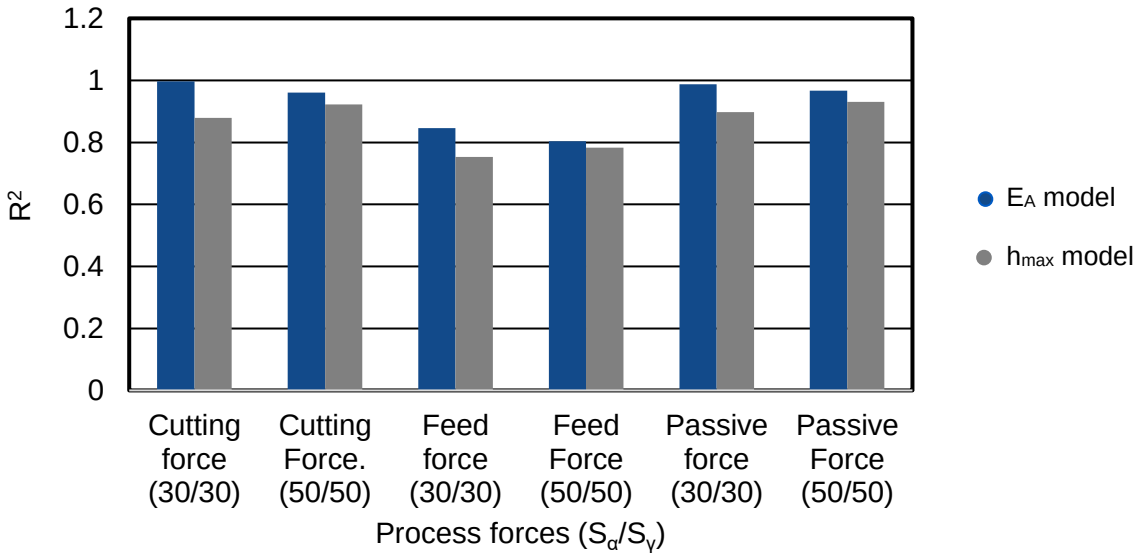

Figure 5.17: Accuracy of the force models.

Table 10 shows the values of the constants for the force model based on the maximum uncut chip thickness. Additionally, the table shows the values of R-squared, which evaluated the quality of the linear regression. As can be seen in Figure 5.17, the values R^2 are lower in all cases compared to the engagement area model, as a result, the h_{max}-based model has less accuracy to predict the process forces as a function of the cutting parameters.

6 Analysis of the influence of the cutting edge shape

6.1 Influence of asymmetric rounding

In order to analyse the influence of asymmetric rounding in process forces, numerous experiments were carried out using ground and tools. Moreover, interrupted cutting tests were conducted to study the behaviour of the tools in discontinuous process. The effect of the microgeometry (S_α and S_γ) in process forces was analysed using depth of cut of 0.1 mm and cutting speed and feed rate are described in Table 11. Four different cutting conditions were tested, and similar results were obtained regarding to the influence of the edge microgeometry. Therefore, only two will be detailed along this document, the lower and the higher cutting parameters (cutting conditions 1 and 4).

Table 11: Cutting parameters

Cutting conditions No.	**1**	**2**	**3**	**4**
Cutting speed (m/min)	160	160	220	220
Feed rate (mm/rev)	0.1	0.2	0.1	0.2
Depth of cut (mm)	0.1	0.1	0.1	0.1

The ground tools described in Table 5 were tested in turning experiments with different cutting parameters. Figure 6.1 shows the different values of cutting and feed forces measured for the different cutting edge microgeometries using a cutting speed of 160 m/min and 0.1 mm/rev.

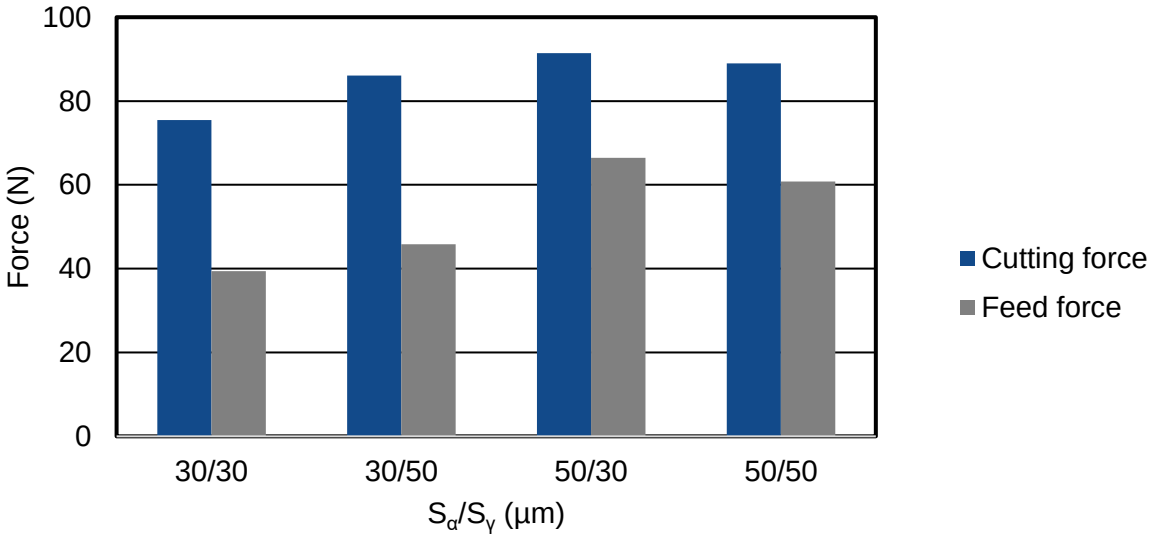

Figure 6.1: Cutting and feed force v_c = 160 m/min / f = 0.1 mm/rev.

As can be seen, the largest values of S_α and S_γ lead to higher process forces, matching with the experimental and numerical analyses performed with other types of steels in the literature [DENK12]. This can be explained because the increase of friction force due to the larger area across the edge. The less sharpness of the cutting tool results in a higher force needed to shear the workpiece material. On the other hand, the results showed a greater influence of S_α on the cutting and feed force. The force needed to shear the material increase with an increasement of S_α. The effect of S_γ was lesser comparing to the flank face segment. This behaviour can be justified because S_α conditions the amount of material that is pressed underneath the flank face. This is known as ploughing effect which affects the new machined surface and the process forces.

About passive forces, the effect of the rake face segment (S_γ) is negligible while S_α has a considerable influence in the force perpendicular to the workpiece axis, as can be seen in Figure 6.2. For the tool with microgeometry of S_α/S_γ = 30/30 µm increasing the S_γ value 30 to 50 µm (tool 2G) leads to an increasement in the force of 22 N, whereas an increasement of S_α (tool 3G) results in an increase of 135 N (108%). The same occurs with the largest symmetrical edge (tool 4G), a reduction of the parameter S_γ results in an insignificant change in the force. However, exist a great decrease when varying S_α.

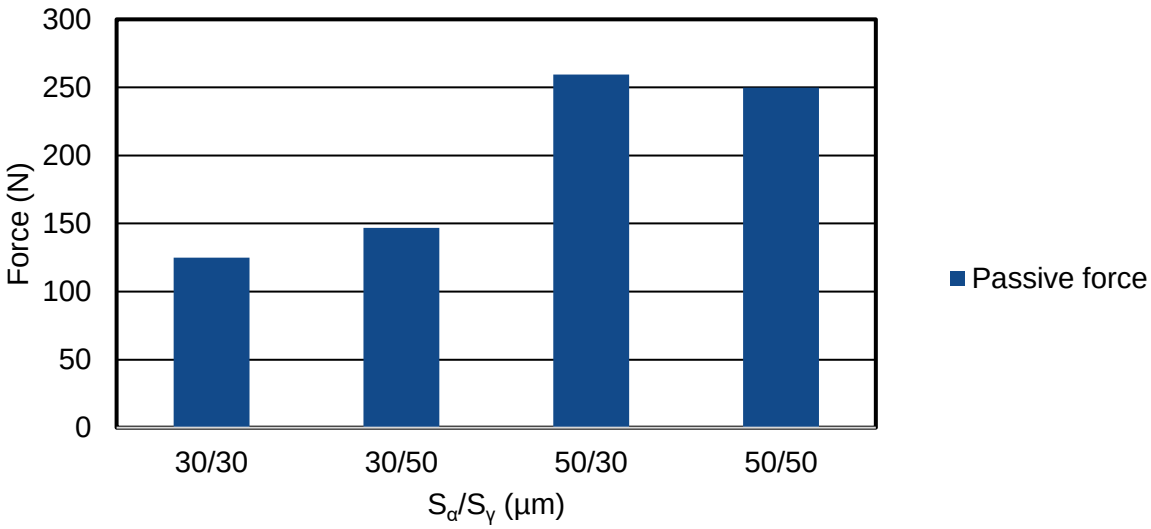

Figure 6.2: Passive force v_c = 160 m/min / f = 0.1 mm/rev.

Agreeing with the literature, the rake flank face segment is the determining factor in the material flow and the size and shape of the stagnation zone, and consequently it will influence the passive force of the process. As well as for cutting and feed force, a symmetrical increasement of S_α and S_γ results on an increasement in the passive force for the reasons mentioned above. On the other hand, as can be seen in the figure

above, the passive component is the highest of the process forces followed by the cutting force. This agrees with the literature like the results found by Bouacha et al. [BOUA10] testing different cutting conditions. The experiments performed with cutting conditions number 4 as shown in Table 11, reported similar results as can be seen in Figure 6.3 and Figure 6.4. Largest microgeometries need higher forces to cut the material. Additionally, varying the value of S_α showed a higher influence in process forces, while S_γ has lesser effect on them. Cutting conditions number 2 and 3 are not shown in this document due to their similar results with conditions 1 and 4.

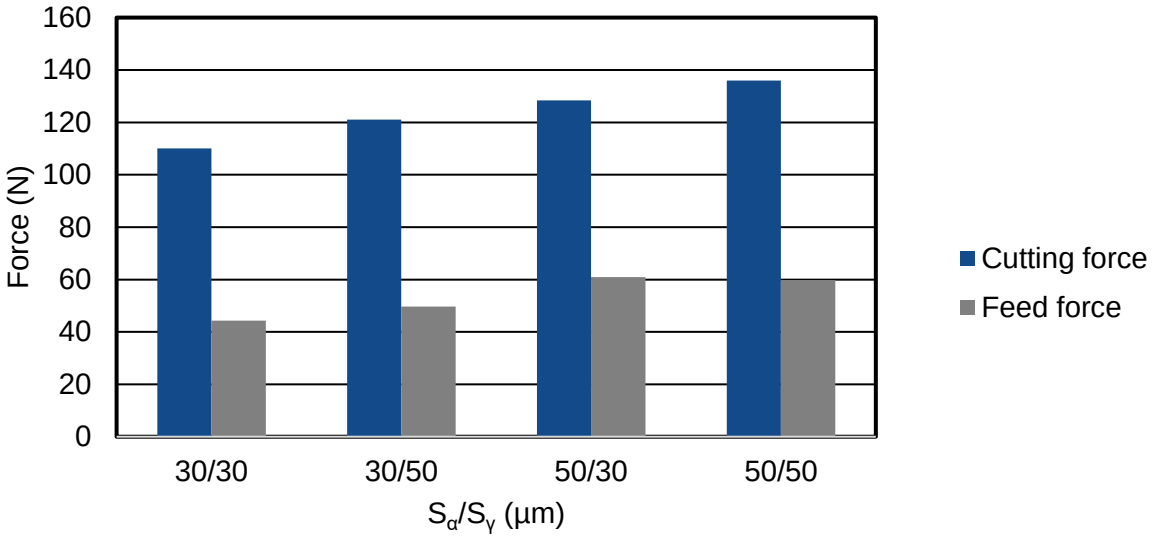

Figure 6.3: Cutting and feed force v_c = 220 m/min / f = 0.2 mm/rev.

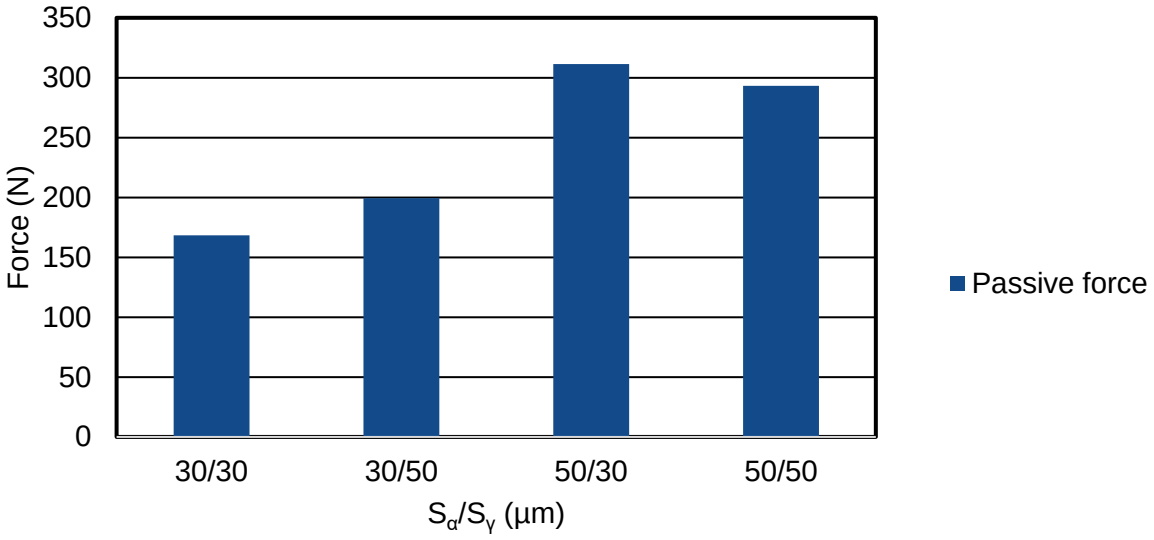

Figure 6.4: Passive force v_c = 220 m/min / f = 0.2 mm/rev.

As can be seen, the process forces of cutting condition 4 are slightly higher comparing to condition 1. This is a consequence of the higher feed rate used (0.2 mm/rev instead of 0.1) despite the fact that a higher cutting speed results in a lower cutting force due to the thermal softening of the material, as was observed during the experiments.

Concerning to interrupted cutting, the ground tools were tested using the cutting parameters of Table 11. Maximum and medium process forces were measured for different cutting speeds and feed rates. Figure 6.5 and Figure 6.7 show the maximum forces measured during the turning process. As can be seen, the max force is higher comparing to the continuous cutting tests using the same cutting conditions and workpiece material. This can be explained because the thermal softening does not appear as it does in continuous cutting. This is due to the cooling of the workpiece while the tool is not in contact with the workpiece. This contributes to a great wear of the edge and a lower tool life comparing to continuous cutting conditions. Only the forces of the cutting parameters v_c = 160 m/min and f = 0.1 mm/rev are analysed in this document because using the other conditions similar results were obtained.

Figure 6.5 shows the maximum values of cutting and feed force. As well as for the continuous cutting situation, the flank face segment (S_α) is the dominant factor in process forces. S_γ showed a much less influence as can be seen in the figures. The largest microgeometries produced higher forces due to the increasement in edge area and friction. An asymmetrical increase of only one of the segments also reported an increase in the forces.

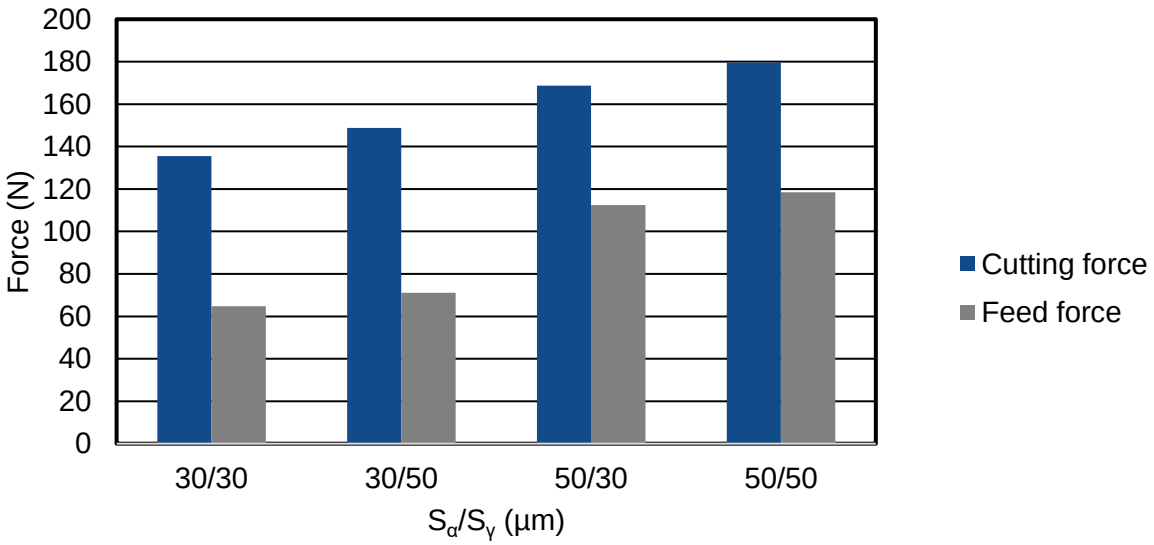

Figure 6.5: Maximum cutting and feed force v_c = 160 m/min / f = 0.1 mm/rev.

For the medium cutting and feed forces, the results found reported a similar influence of the rake and flank face segments (Figure 6.6). In addition, the increase of one of the segments (S_α and S_γ) showed an increasement of the process forces as a consequence of the higher size of one of the segments.

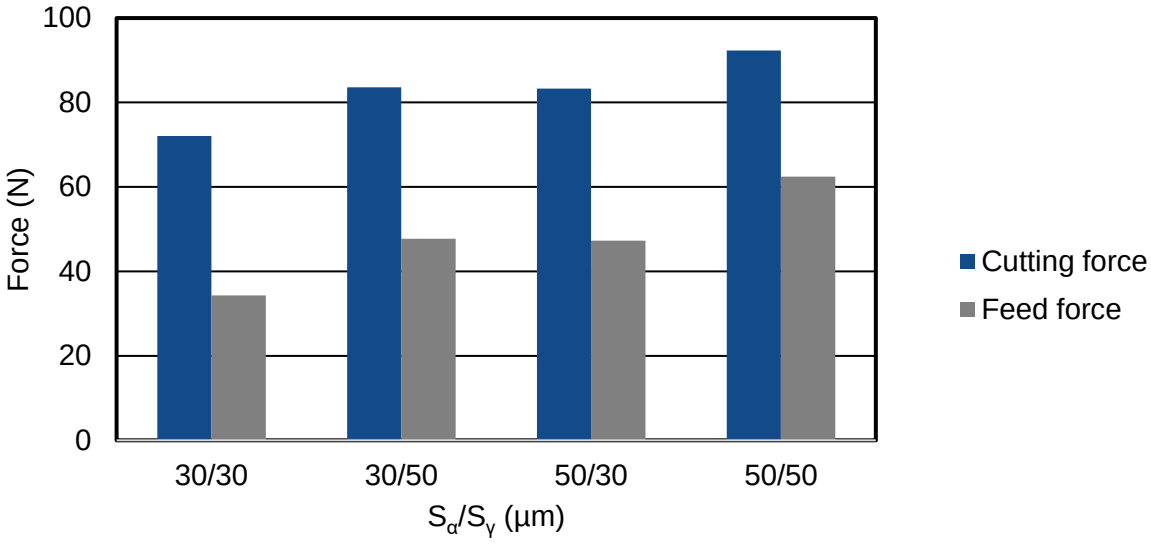

Figure 6.6: Medium cutting and feed force v_c = 160 m/min / f = 0.1 mm/rev

Regarding to maximum passive forces, the influence of the rake face segment is again almost negligible. On the other hand, S_α showed a high effect on the force. Between tool 1G and 3G exist a great difference in the force because S_α change its value from 30 to 50 µm, whereas a change of S_γ from 30 to 50 µm (tool 1G and 2G) causes a smaller variation of the passive force (Figure 6.7).

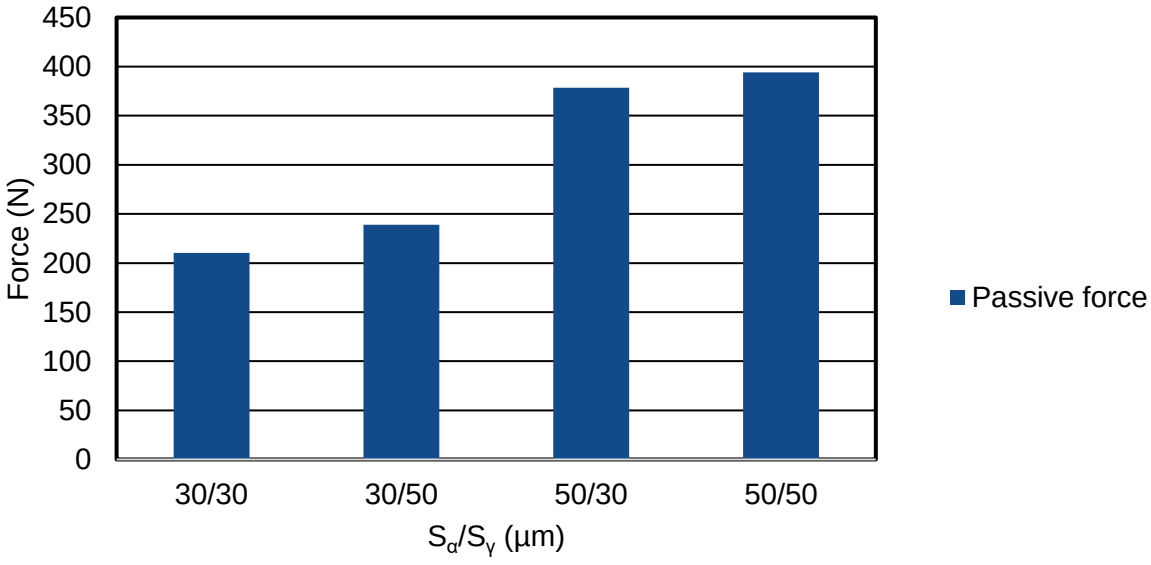

Figure 6.7: Maximum passive force v_c = 160 m/min / f = 0.1 mm/rev

The measures of medium passive force reported a high influence of both cutting segments, similar to medium cutting and feed forces. However, S_α showed the greater impact on the force, but S_γ had a considerable effect (Figure 6.8).

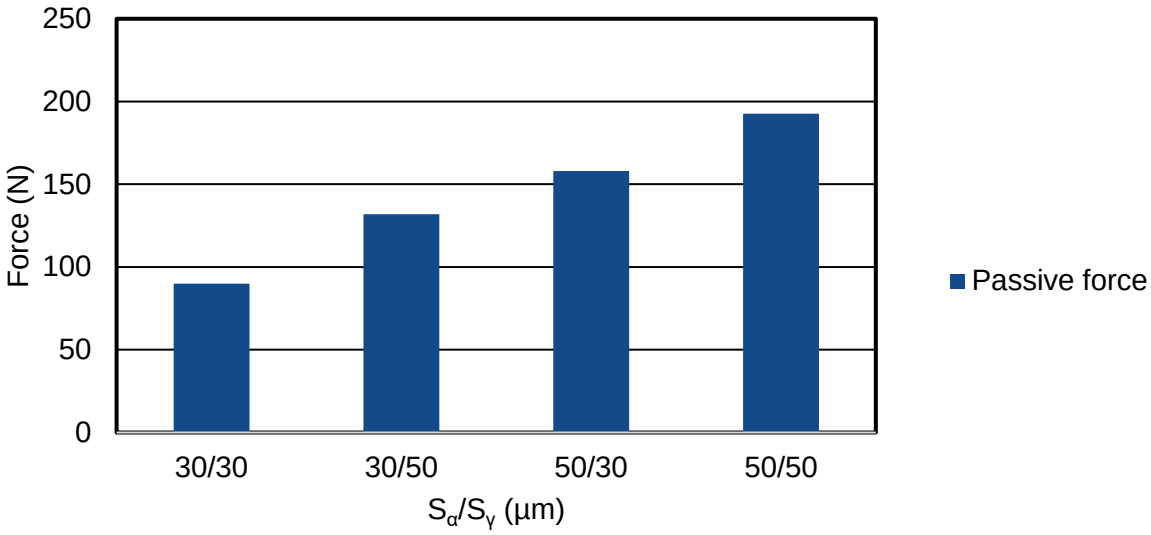

Figure 6.8: Medium passive force v_c = 160 m/min / f = 0.1 mm/rev

The force model developed in previous chapter, has been calculated with force measurements obtained with symmetrical edges. In order to develop a general model for both symmetric and asymmetric microgeometries, new constants have been interpolated using the average cutting edge rounding, which is the average length of the rake and flank face segments. The new constants are described in Table 12.

Table 12: Constants for the engagement area model for S_α/S_γ = 40/40 µm

	Cutting Force	Feed Force	Passive force
M	4895.6	3161	5149.65
N	30.525	28.75	190.44

Figure 6.9 shows the values of process forces calculated using the engagement area model and the microgeometry S_α/S_γ = 40/40 µm. The figure shows a comparation with the values measured of the tools with the geometry S_α/S_γ = 30/50 µm and S_α/S_γ = 50/30 µm. As can be seen, the edge with geometry S_α/S_γ = 50/30 µm reported a more accurate approximation to the estimated values using the model. Figure 6.11 shows the relative error for both asymmetrical microgeometries, as can be seen the geometry S_α/S_γ = 50/30 µm reported a lower error, this can be explained due to the higher influence that S_α has on the process forces, as commented in previous chapters. On the other hand, both asymmetric geometries presented the same value of average edge

rounding but the experiments reported different values of the forces, which in incompatible for the developed force model, therefore it needs further investigation.

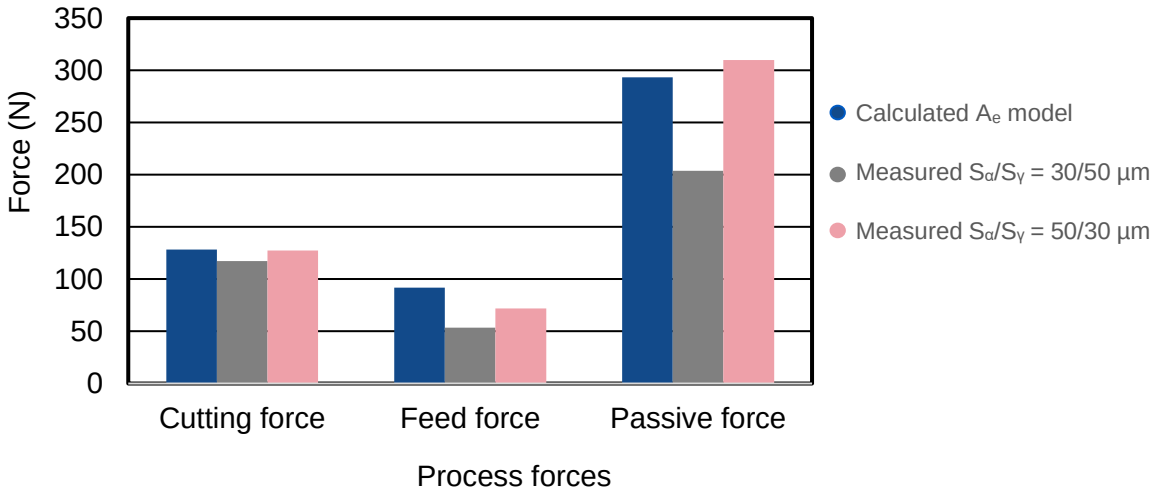

Figure 6.9: Process forces for A_e = 0.01 mm^2.

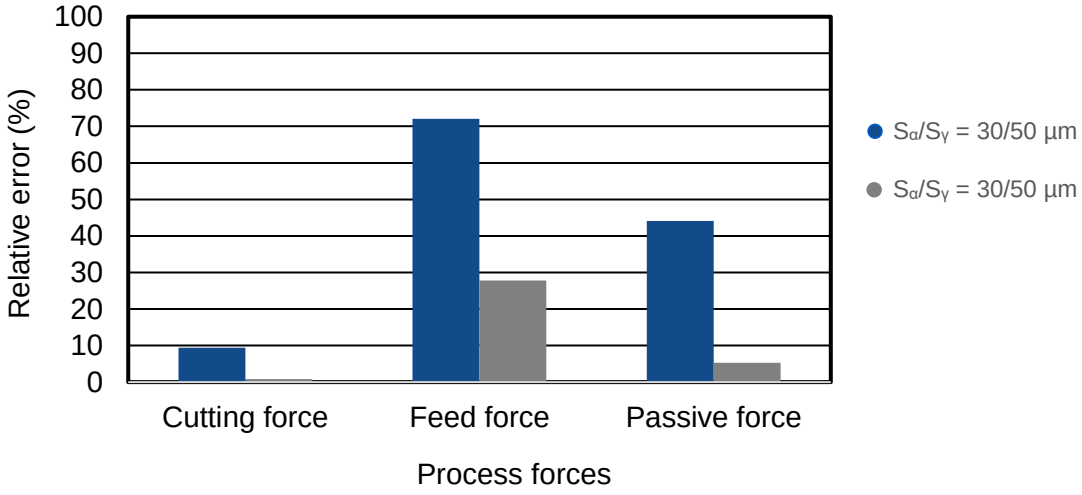

Figure 6.10: Relative error for the asymmetric geometries.

6.2 Influence of continuous rounding

Regarding to continuous rounding, the brushed tools described in Table 4 were tested in continuous turning experiments with different cutting parameters. The first experiments were carried out in order to analyse the influence of the microgeometry (S_α and S_γ) in process forces for continuous cutting. The depth of cut used was 0.1 mm and cutting speed and feed rate are described in Table 11, the same as for the ground

tools. Four different cutting conditions were tested, and similar results were obtained regarding to the influence of the edge microgeometry.

Brushed tools reported similar results as the ground tools. As can be seen in Figure 6.11 and Figure 6.12, S_α was the determinant factor in process forces which agrees with the results obtained with ground tools with the particularity that there is less difference in the effect of the two segments (S_α and S_γ). Additionally, in the figures can be seen the low forces the sharp edge of tool with microgeometry of S_α/S_γ = 15/15 µm needs to shear the workpiece material. On the other hand, similar results were obtained for the cutting conditions number 2, 3 and 4, therefore the figures of the results are not shown in this document.

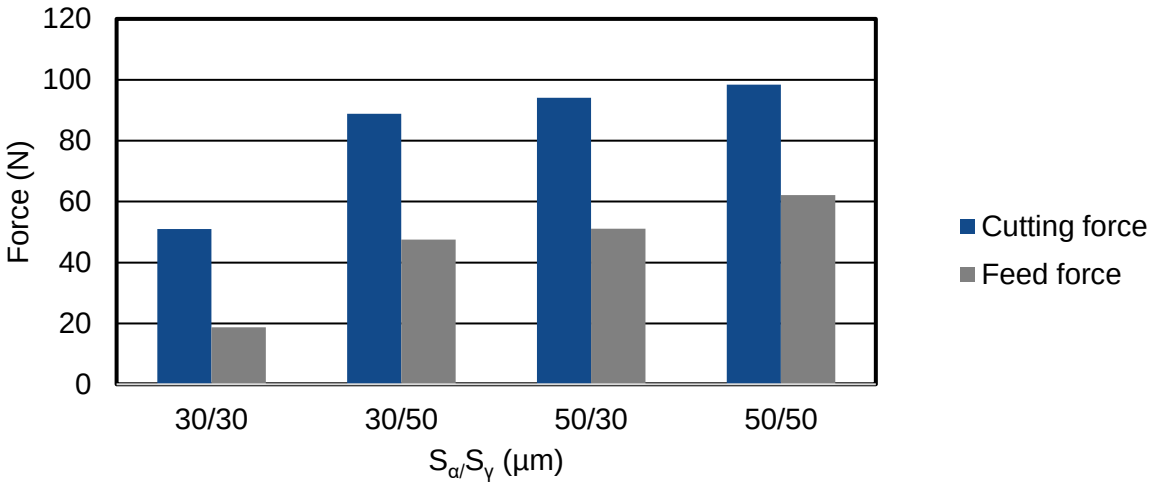

Figure 6.11: Cutting and feed force v_c = 160 m/min / f = 0.1 mm/rev. Brushed tools.

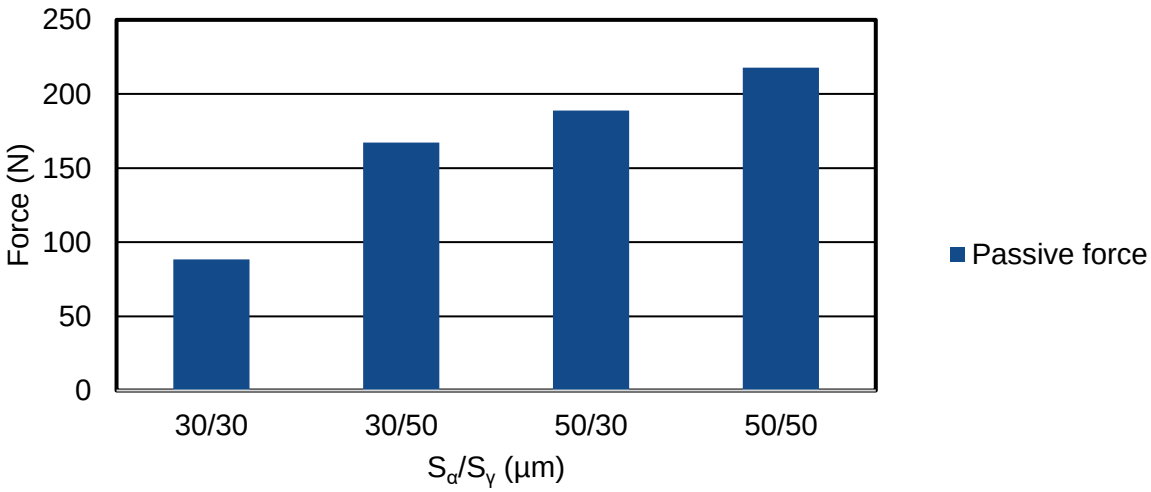

Figure 6.12: Passive force v_c = 160 m/min / f = 0.1 mm/rev. Brushed tools.

6.3 Influence of tool wear

Due to the high mechanical and thermal loads resulting when machining hardened steel, the tools suffer a pronounced wear that mainly is crater and flank wear. The objective of this chapter is to analyse the effect of the wear in the process forces. As it is well known, the wear of the edge tends to increase the size of the edge rounding, and as was described in previous sections in this document, larger edge microgeometries produced higher forces needed to shear the workpiece material. Two different cutting conditions were tested achieving similar results. These are described in Table 11, conditions number 1 and 4 were used. The following figure will describe the variation in process forces using cutting condition number 1 (v_c=160 m/min, f=0.1 mm/rev).

Figure 6.13 shows the variation of the process forces between a new and a worn tool. The tool 1G has the smaller edge microgeometry, therefore the wear will produce a great increasement in the size of the edge rounding. This will cause an increase in the forces as can be seen in the graph below.

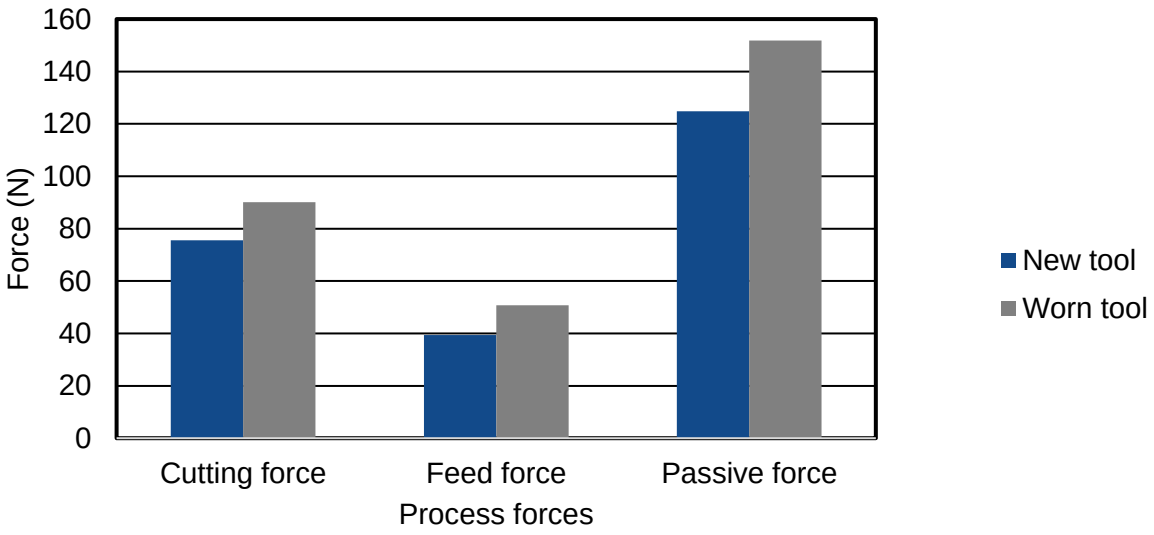

Figure 6.13: Variation of the force of tool with microgeometry of S_α/S_γ = 30/30 µm.

The asymmetric edges (tools 2G and 3G) reported different results in regard to the forces of new and worn tools. Figure 6.14 and Figure 6.15 describe the variation in the forces for the asymmetric edges. For tools 1G (S_α/S_γ = 30/30 µm) and 2G (S_α/S_γ = 30/50 µm) there is practically no difference between them, both reported a high variation of the force. This is due to the small influence that Sγ has on the process forces as was commented before in this document. On the other hand, tool 3G (S_α50/S_γ30)

reported a big variation between the worn and the new tool. This can be explained because the big effect S_α has on the process forces.

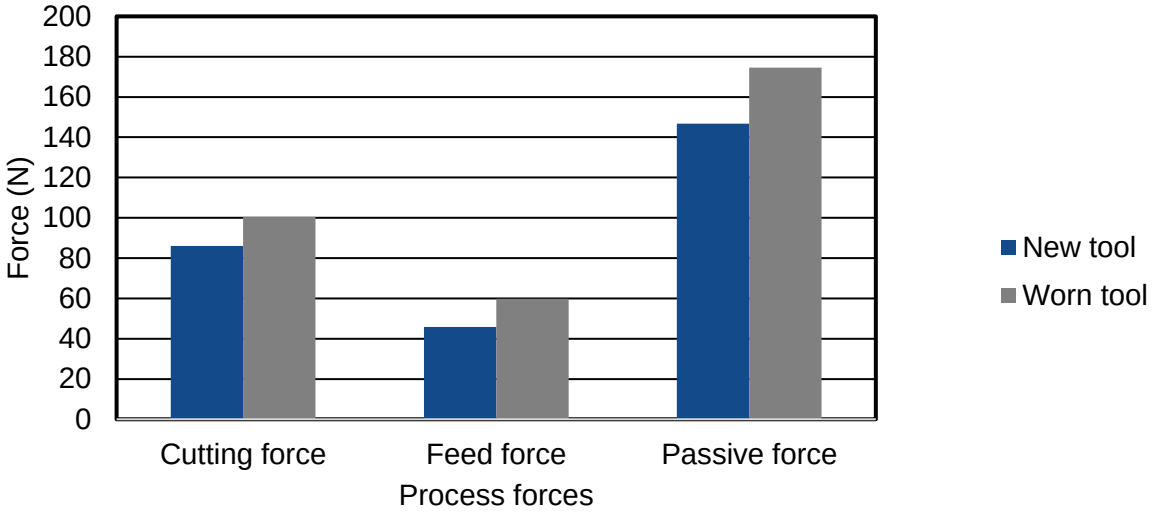

Figure 6.14: Variation of the force of tool 2G (S_α/S_γ = 30/50 µm).

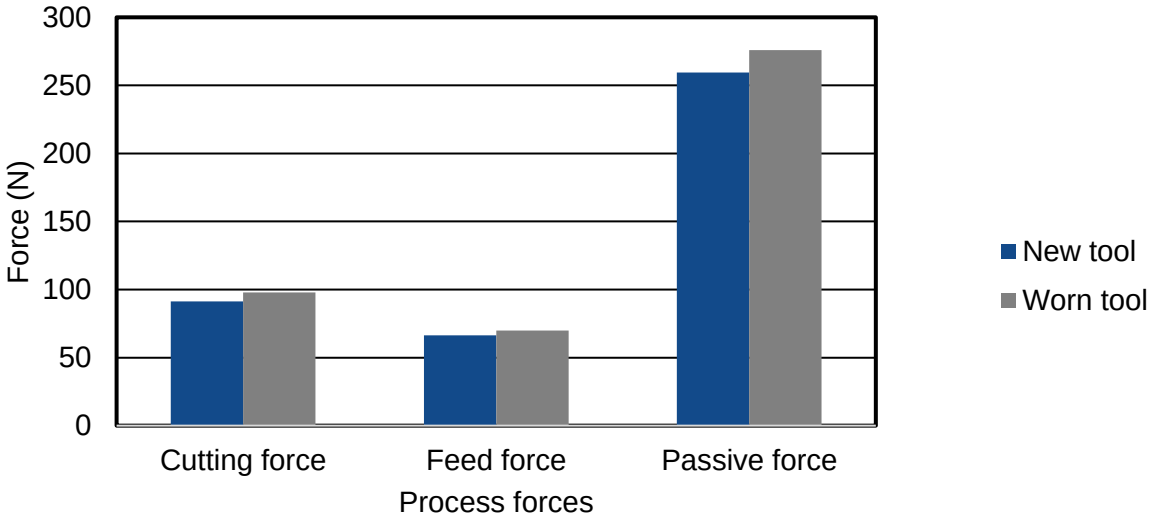

Figure 6.15: Variation of the force of tool 3G (S_α/S_γ = 50/30 µm).

Finally, for the biggest symmetric microgeometry, exist a small different between the new and the worn tool, being higher the force of the worn one as can be seeing in Figure 6.16. An increase of S_γ from 30 to 50 µm does not produce any significant change. As was commented before, the bigger microgeometries, suffer less variation in the size of the rounding of their edges due to tool wear, consequently, these tools will not need significant increase in the forces to shear the material.

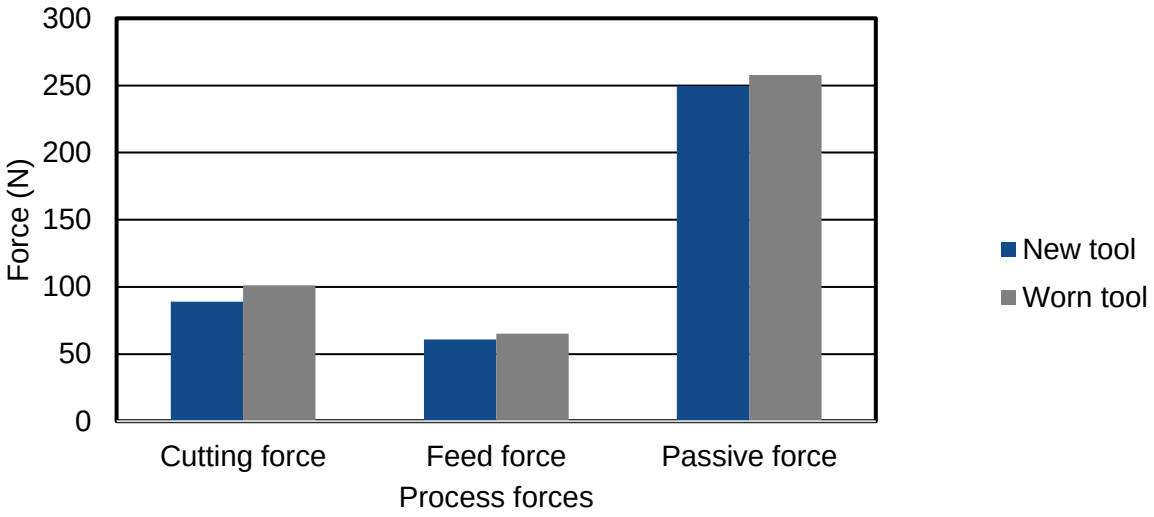

Figure 6.16: Variation of the force of tool 4G (S_α/S_γ = 50/50 µm).

6.4 Analysis of the machined surfaces

With the purpose of analyse the influence of the shape of edge microgeometry on surface quality, numerous continuous cutting tests were carried out, as well as surface roughness measurements. For the ground tools, show the values of surface roughness (R_a and R_z) achieved during continuous cutting tests with the following process parameters: v_c = 160 m/min, f = 0.1 mm/rev and a_p = 0.1 mm. In both figures below con be seen that shaper edges produce a better surface quality whereas the bigger microgeometry achieved high values of R_a and R_z. This can be explained because the high deformation of the machined surface when using big rounding edges, this is caused by all the material that is pressed underneath the flank face. On the other hand, sharper edges barely deform the new surface, therefore higher surface qualities can be reached. This agrees the results reported by the literature, for example the numerical analyses performed by Denkena et al. [DENK12].

Concerning to asymmetrical microgeometries, in Figure 6.17 can be seen the influence of S_α and S_γ on the surface roughness. S_α reported the higher effect on R_a and R_z whereas S_γ had a much less influence on it. This is due to fact that S_α is the determinant factor in material flow, it affects the amount of material which flows underneath the flank face, consequently, is the parameter that controls the surface roughness achieved. These results agree with the test carried out by the literature [DENK12]. For bigger values of S_α, more material is pressed under the flank face, consequently the roughness rises. S_γ has a negligible effect on material flow, therefore it has a small effect on surface roughness.

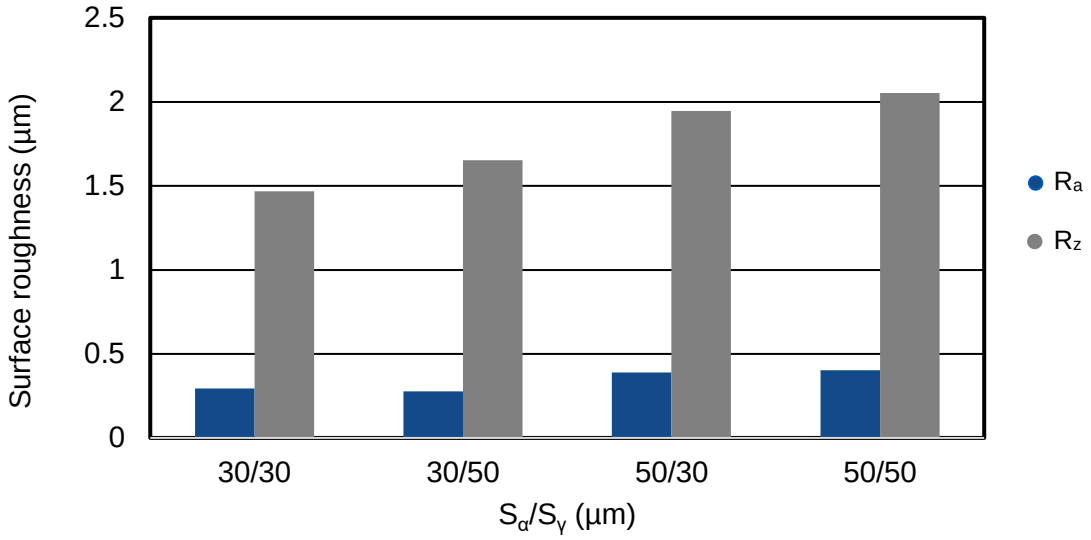

Figure 6.17: Surface roughness for different edge microgeometries. Ground tools.

Concerning to brushed tools, the surface roughness was evaluated to analyse the influence of shape of the cutting edge when using continuous rounding tools. Figure 6.18 shows the values of the surface roughness achieved with process parameters: v_c = 160 m/min, f = 0.1 mm/rev and a_p = 0.1 mm. As for the ground tools, S_α was the parameter that genuinely influence the roughness of the machines surface. However, for the brushed tools S_γ has a higher effect in R_a and R_z in contrast to ground tools.

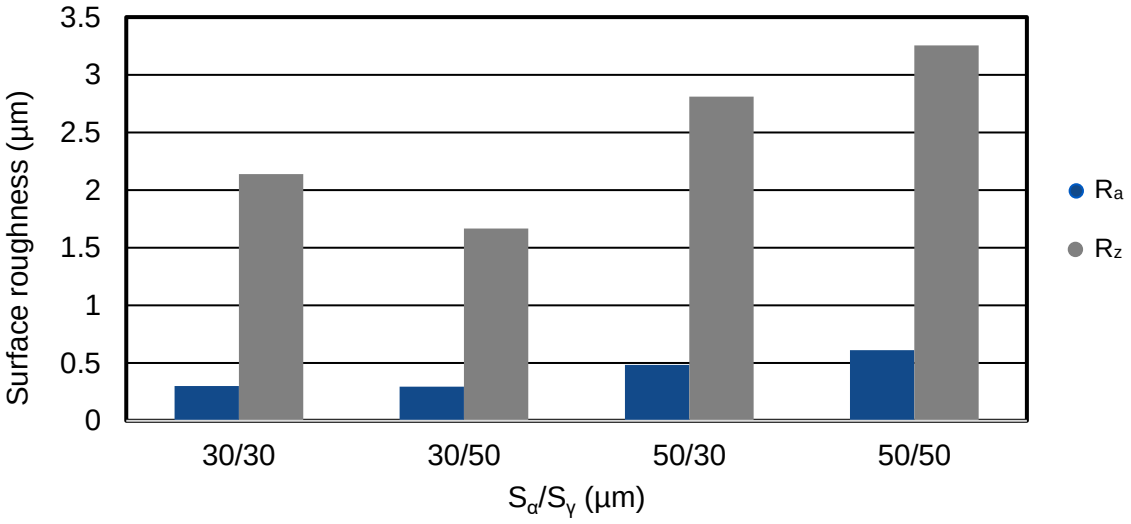

Figure 6.18: Surface roughness for different edge microgeometries. Brushed tools.

7 Analysis of chip formation

Chip segmentation and saw-toothed chips are common in hard machining due to thermomechanical instabilities which occur during the cutting process. In order to describe this phenomenon, a parameter called degree of segmentation (G_s) is used to quantify the segmentation (Figure 7.1). It is the ratio between the length of the valley and the peak of the saw-toothed chip. The chips were subjected to a polishing process to obtain their cross section and analyse the segmentation under the microscope.

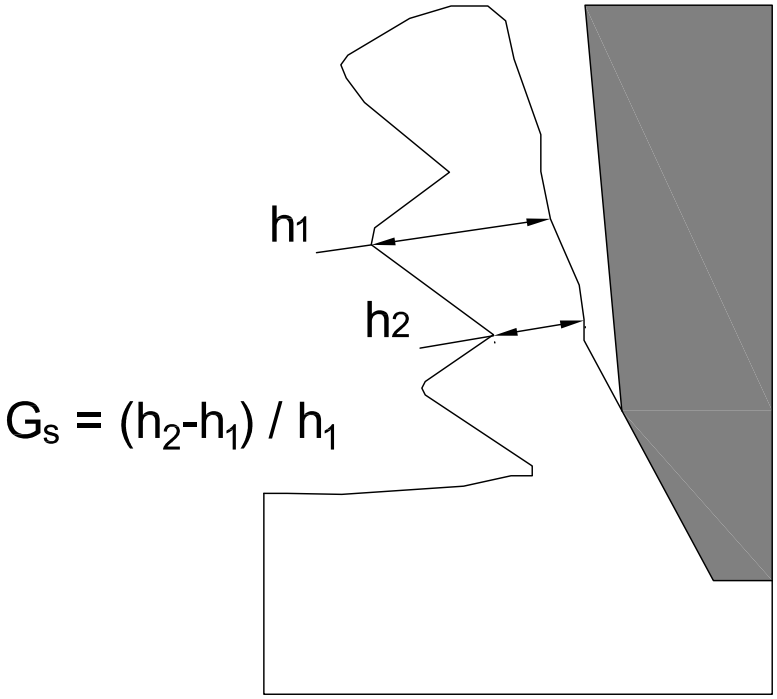

Figure 7.1: Degree of segmentation [DENK21].

7.1 Influence of the cutting edge shape

In order to study the influence of the shape of the cutting edge, numerous chip formation analyses have been carried out. Different cutting edge preparations and symmetric and asymmetric rounding have been tested.

Firstly, the ground tools have been analysed. Figure 7.2 shows the section of the chips obtained with edges S_α/S_γ = 30/30 µm and S_α/S_γ = 30/50 µm. The degree of segmentation measured was 0.71 for the smaller microgeometry. As can be seen the value of the degree of segmentation for the edge S_α/S_γ = 30/50 is higher comparing to the symmetrical edge. It reaches the value of 0.89. The microgeometry S_α/S_γ = 50/50 reported

a degree of segmentation of 0.79, which means that a symmetrical increase of the size of the edge lead to an increase of chip segmentation. This can be explained due to the higher stresses applied on the material. Chip segmentation is caused by thermomechanical instabilities, therefore higher stresses will produce an increasement in chip segmentation.

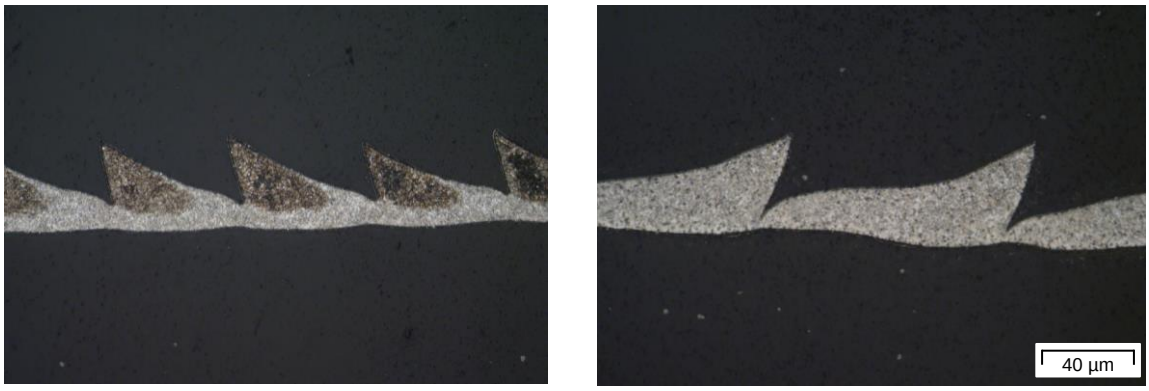

Figure 7.2: Chip sections of tool with microgeometry of S_α/S_γ = 30/30 (left) and S_α/S_γ = 30/50 µm (right). v_c = 160 m/min, f = 0.1 mm/rev and a_p = 0.1.

Regarding to brushed tools, the chip segmentation was examined under the microscope and the degree of segmentation was calculated using a measuring software as shown in Figure 7.1. The symmetrical tools reported a degree of segmentation of 0.65 and 0.68 for the tools with the microgeometry of S_α/S_γ = 15/15 µm and S_α/S_γ = 50/50 µm respectively, the chip segmentation was higher for the edges with the bigger rounding. These results agree with those obtained for the ground tools.

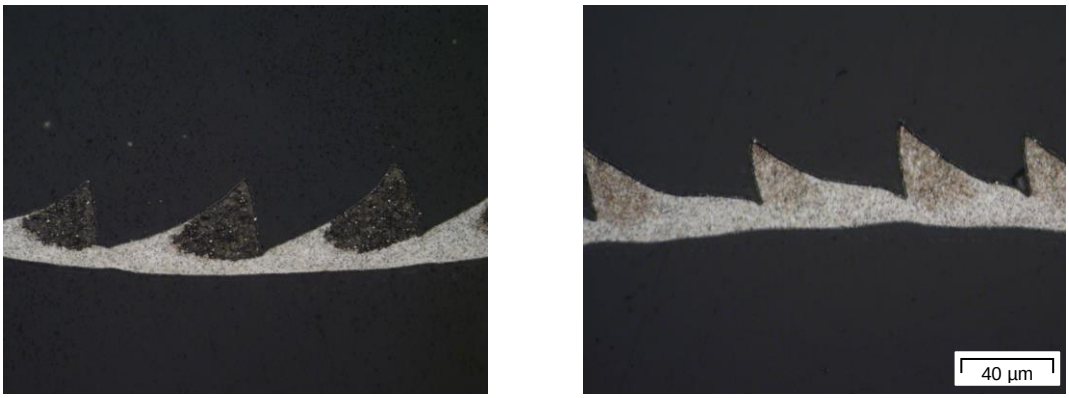

Figure 7.3: Chip section of tool with microgeometry of S_α/S_γ = 30/50 µm (left) and S_α/S_γ = 50/30 µm (right). v_c = 160 m/min, f = 0.1 mm/rev and a_p = 0.1.

Concerning to the asymmetrical edges, according to the ground tools, the analysis reported more segmented chips reaching the average values of 0.82 and 0.75 for tool with microgeometry of S_α/S_γ = 30/50 µm and S_α/S_γ = 50/30 µm respectively, as shown in Figure 7.3.

All the values of the average degree of segmentation are resumed in Figure 7.4 for the different ground and brushed tools. As can be seen, the value of the degree of segmentation is always lower for the ground tools. In addition, it can be stated that bigger microgeometries cause more chip segmentation due to the higher stresses applied to the material.

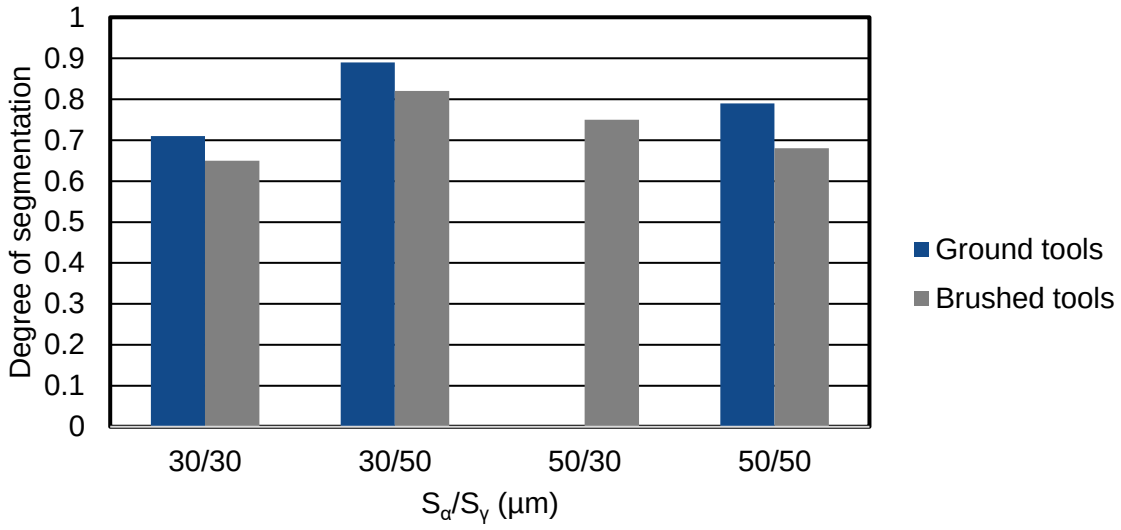

Figure 7.4: Degree of segmentation as a function of the shape of the cutting edge

7.2 Influence of cutting parameters

With the aim of analysing the effect of cutting speed and cutting depth in chip formation and chip segmentation, several experiments were performed using the symmetrical ground tools with microgeometry of S_α/S_γ = 30/30 and S_α/S_γ = 50/50 µm. Firstly, the variation of cutting depth was analysed using the values of 0.05, 0.1, 0.2 and 0.3 mm, v_c = 160 m/min and f = 0.1 mm/rev. Figure 7.5 (left) shows the section of the chip obtained using tool S_α/S_γ = 50/50 and a cutting depth of 0.1 mm, the degree of segmentation measured was 0.64. Figure 7.5 (right) shows the chip obtained a depth of cut of 0.3 and a degree of segmentation of 0.77.

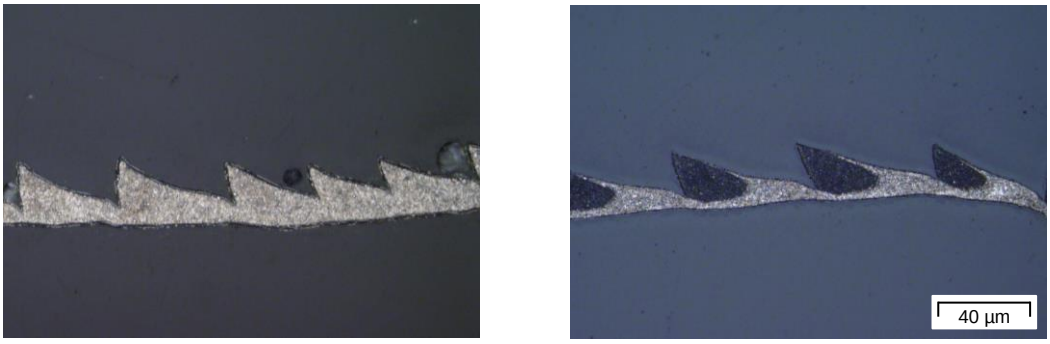

Figure 7.5: Chip section of tool with microgeometry of S_α/S_γ = 50/50 µm. v_c = 160 m/min, f = 0.1 mm/rev, a_p = 0.1 (left) and a_p = 0.3 (right).

Figure 7.6 shows the values of the degree of segmentation as a function of the cutting depth. As can be seen, the degree of segmentation increases with the increase of cutting depth for both geometries. This can be explained due to the fact that the stress on the material rises when the cutting depth is increased. It leads to an increasement in chip segmentation. As was commented in previous chapter, the biggest rounding leads to a higher degree of segmentation.

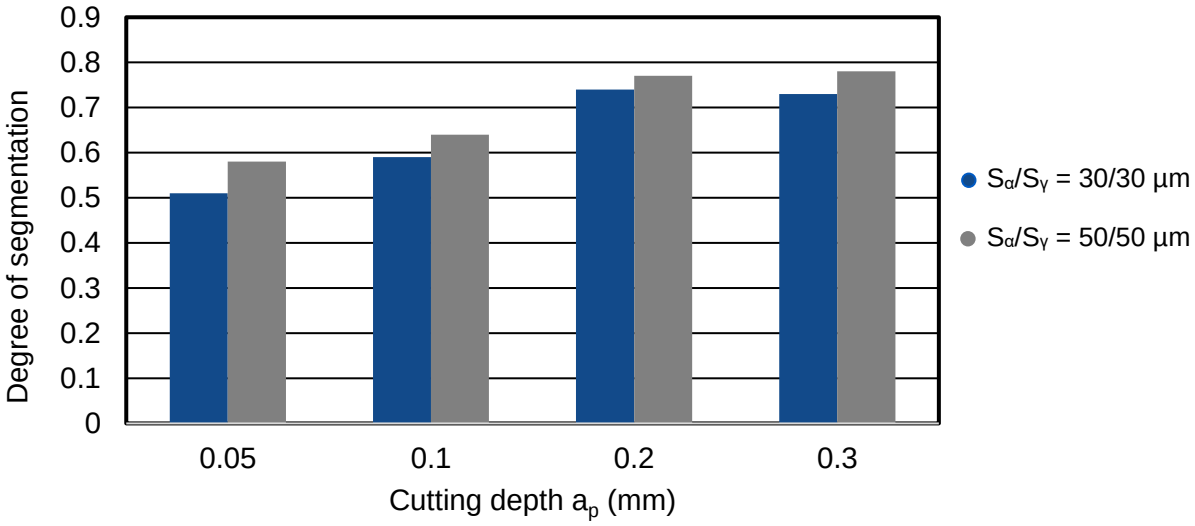

Figure 7.6: Degree of segmentation as a function of the cutting depth

Regarding to the influence of cutting speed in chip formation, numerous tests were carried out with the values of cutting speed of 50, 100 and 200 m/min, and a_p = 0.2 and f = 0.1 for the tools with the microgeometry of S_α/S_γ = 30/30 and S_α/S_γ = 50/50 µm. In Figure 7.7 shows the saw-toothed chip obtained with v_c = 100 m/min (left) and v_c = 200 m/min (right) for the smaller edge microgeometry.

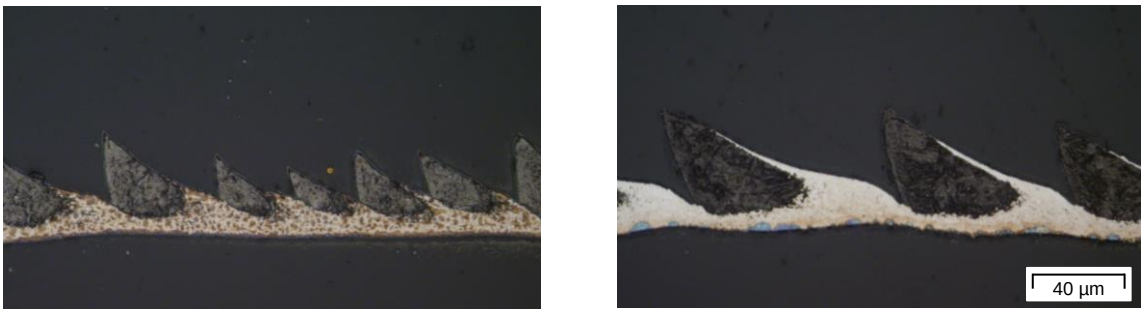

Figure 7.7: Chip section of tool with microgeometry of S_α/S_γ = 30/30 µm. f = 0.1 mm/rev, a_p = 0.2, v_c = 100 m/min (left) and v_c = 200 m/min (right).

In Figure 7.8 can be observed the influence of cutting speed in chip formation for both edge microgeometries. The increase of cutting speed leads to an increase in chip segmentation due to the higher temperature reached at the edge when the cutting speed rises, consequently the chip segmentation increases. Note that the tool 4G does not have a value for v_c = 200 m/min due to a failure occurred during the polishing process.

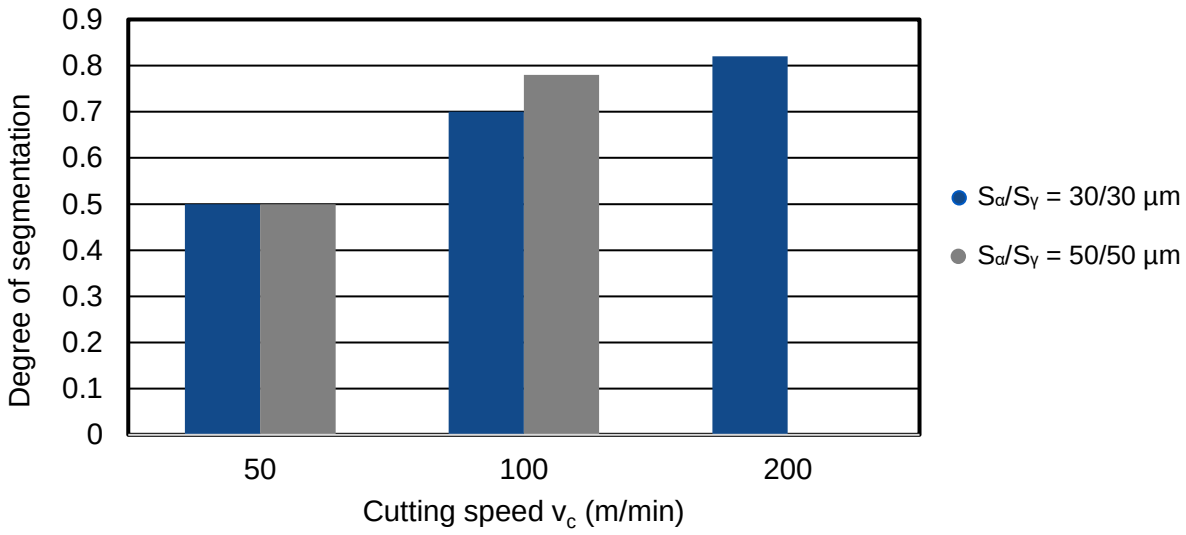

Figure 7.8: Degree of segmentation as a function of the cutting speed.

8 Conclusions and future research lines

8.1 Conclusions

Along this thesis the influence of edge microgeometry and process parameters in cutting forces, chip formation and surface roughness has been analysed obtaining the following conclusions.

Firstly, the influence of process parameters was studied. Cutting speed has a linear dependency with process forces. The results reported a decrease of the force with an increase of cutting speed. This is due to the thermal softening of the material as consequence of the increasing cutting temperature for higher cutting speeds. Moreover, the biggest rounding reported higher process forces. Feed rate and cutting depth described a linear relation with process forces. As expected, higher values of both produced an increasement of process forces. Again, the biggest edge microgeometry produced higher cutting forces. With the aim of predict the cutting forces as a function of the feed rate and cutting depth, two different models have been developed. Two methods were employed, the engagement area (A_e) and the maximum uncut chip thickness (h_{max}), showing that the engagement area is more suitable to estimate the forces due to its higher accuracy.

Regarding to the influence of the shape of the cutting edge, it was found that S_α is the parameter which influence the most in process forces and surface roughness for ground and brushed tools, being S_γ almost negligible for continuous and interrupted cutting. Higher values of S_α produce lower quality of the machined surfaces and higher process forces as a consequence of the higher friction and the amount of material which is pressed underneath the flank face. The force model applied to asymmetrical edges reported that the microgeometries with higher S_α showed lower relative error between the measurements and the estimated values. This is due to the influence that this parameter has on process forces. On the other hand, the analysis of tool wear has showed that the variation of the cutting forces produced on the worn tools is more pronounced for less rounded edges. This is caused by the rapid wear suffered by the sharp edges, as a consequence these edges become more rounded, which produces an increase in cutting forces.

Finally, as regards to chip formation, it can be stated that it is conditioned by the size of the cutting edge rounding. An increase of edge rounding caused an increase of the degree of segmentation. This is due to the higher stresses that are applied on the material when the size of the rounding is increased. Moreover, cutting speed and cutting depth influence the chip formation. The increasement of the two parameters leads

to an increase of the degree of segmentation. This is caused by the rise of the cutting temperature and material stresses when increment the value of the cutting parameters.

8.2 Futures research lines

In the present document, chip formation, process forces quality of the machined surface when turning AISI 52100 have been analysed as a function of cutting edge microgeometry and process parameters (cutting speed, feed rate and cutting depth). Moreover, a force model has been developed in order to predict the process forces for the symmetrical tools with an edge preparation of grinding. As showed in previous chapters, the asymmetrical edges with higher S_α values fitted the model, in contrast with the edges with higher S_γ. Therefore, an interesting future line of investigation would be perform turning experiments using those edges and extrapolate a curve. A general force model for both symmetrical and asymmetrical tools would be obtained.

Regarding to chip formation, a numerical analysis using FEM software would be suitable to study the microscopy interaction between the tool edge and the workpiece material. Additionally, the thermal tool load can be analysed using this technique. The thermomechanical results found in the simulations would be interesting to precisely study how the chip is formed during the machining operations. On the other hand, the relation between cutting edge microgeometry and tool life has not been analysed, consequently, analyse the wear of the tools used during the experiments would be useful to find the most suitable microgeometry.

9 Literature

[DENK11] Denkena, B.; Tönshoff, H.K. (2011) Spanen: Grundlagen, Springer Verlag, Heidelberg

[GODO11] De Godoy, V. A. A., & Diniz, A. E. (2011). Turning of interrupted and continuous hardened steel surfaces using ceramic and CBN cutting tools. Journal of Materials processing technology, 211(6), 1014-1025.

[KLOC05] Klocke, F., Brinksmeier, E., & Weinert, K. (2005). Capability profile of hard cutting and grinding processes. CIRP annals, 54(2), 22-45.

[BOUA10] Bouacha, K., Yallese, M. A., Mabrouki, T., & Rigal, J. F. (2010). Statistical analysis of surface roughness and cutting forces using response surface methodology in hard turning of AISI 52100 bearing steel with CBN tool. International Journal of Refractory Metals and Hard Materials, 28(3), 349-361.

[ABRA93] Abrão, A.M., Aspinwall, D.K., Wise, M.L.H. (1993). A review of polycrystalline cubic boron nitride cutting tool developments and application. In: Kochhar, A.K. (eds) Proceedings of the Thirtieth International

[SADI12] Sadik, M. I. (2012). Wear development and cutting forces on CBN cutting tool in hard part turning of different hardened steels. Procedia Cirp, 1, 232-237.

[CHOU99] Chou, Y. K., & Evans, C. J. (1999). Cubic boron nitride tool wear in interrupted hard cutting. Wear, 225, 234-245.

[DENK05] Denkena, B., Becker, J. C., & de Leon-Garcia, L. (2005, May). Study of the influence of the cutting edge microgeometry on the cutting forces and wear behaviour in turning operations. In Proceedings of the 8th CIRP, International Workshop on Modelling of Machining Operations, Chemnitz, Germany (pp. 503-507).

[ZHOU03] Zhou, J. M., Walter, H., Andersson, M., & Stahl, J. E. (2003). Effect of chamfer angle on wear of PCBN cutting tool. International Journal of Machine Tools and Manufacture, 43(3), 301-305.

[DENK14] Denkena, B., & Biermann, D. (2014). Cutting edge geometries. CIRP annals, 63(2), 631-653.

[DENK21] Denkena, B., Krödel, A., & Heckemeyer, A. (2021). Numerical and experimental analysis of thermal and mechanical tool load when turning AISI 52100 with ground cutting edge microgeometries. CIRP Journal of Manufacturing Science and Technology, 35, 494-501.

[DENK12] Denkena, B., Köhler, J., & Mengesha, M. S. (2012). Influence of the cutting edge rounding on the chip formation process: Part 1. Investigation of material flow, process forces, and cutting temperature. Production engineering, 6(4), 329-338.

[BARR02] Barry, J., & Byrne, G. (2002). The mechanisms of chip formation in machining hardened steels. J. Manuf. Sci. Eng., 124(3), 528-535.

[UMBR04] Umbrello, D., Hua, J., & Shivpuri, R. (2004). Hardness-based flow stress and fracture models for numerical simulation of hard machining AISI 52100 bearing steel. Materials Science and Engineering: A, 374(1-2), 90-100.

[ELBE96] Elbestawi, M. A., Srivastava, A. K., & El-Wardany, T. I. (1996). A model for chip formation during machining of hardened steel. CIRP annals, 45(1), 71-76.

[TIFF19] Tiffe, M., Saelzer, J., & Zabel, A. (2019). Analysis of mechanisms for chip formation simulation of hardened steel. Procedia CIRP, 82, 71-76.

[ZHAO17] Zhao, T., Zhou, J. M., Bushlya, V., & Ståhl, J. E. (2017). Effect of cutting edge radius on surface roughness and tool wear in hard turning of AISI 52100 steel. The International Journal of Advanced Manufacturing Technology, 91(9), 3611-3618.

[DENK10] Denkena, B., de Leon, L., Bassett, E., & Rehe, M. (2010). Cutting edge preparation by means of abrasive brushing. In Key Engineering Materials (Vol. 438, pp. 1-7). Trans Tech Publications Ltd.

[VENT13] Ventura, C. E. H., Köhler, J., & Denkena, B. (2013). Cutting edge preparation of PCBN inserts by means of grinding and its application in hard turning. CIRP Journal of Manufacturing Science and Technology, 6(4), 246-253.

[DENK13] Denkena, B., Köhler, J., & Ventura, C. E. H. (2013). Customized cutting edge preparation by means of grinding. Precision Engineering, 37(3), 590-598.